A LISFLOOD-FP hydraulic model of the middle reach of the Congo

F.E. O'Loughlin[1,2] J. Neal[2], G.J.P. Schumann[2,3], E. Beighley[4] & P.D. Bates[2]

[1] Dooge Centre for Water Resources Research, School of Civil Engineering, University College Dublin, Dublin, Ireland

[2] School of Geographical Sciences, University of Bristol, Bristol, BS8 1SS, UK

[3] Remote Sensing Solutions, Inc., Monrovia, CA 91016, USA

[4] Civil and Environmental Engineering, Northeastern University, Boston, MA 02115, USA

Correspondence to:

Fiachra O'Loughlin,

Dooge Centre for Water Resources Research, School of Civil Engineering, University College Dublin, Dublin, Ireland

E-mail: fiachra.oloughlin@ucd.ie

Phone: +353 1 7163222

Abstract:

In this paper we attempt to produce a first hydrodynamic model of the middle reach of the Congo river system in order to understand what controls this river's unique bimodal flood pulse. The model covers the area between Kisangani and Kinshasa on the main stem and includes the major tributaries and the Cuvette Centrale wetland, one of the world's largest and most understudied lowland regions. A mixture of in-situ discharges and modelled discharge from a basin-wide catchment hydrology model were used to force a four-kilometre resolution hydrodynamic simulation developed using the LISFLOOD-FP model. River channels are represented as sub-grid scale features and their width is therefore decoupled from that of the over-lying floodplain grid. Unknown channel friction and bathymetry parameters were calibrated using ERS-2 and Envisat satellite altimetry measurements of channel water level. The calibrated model simulated channel water surface elevations across the domain with a bias and root mean square error of 0.185 and 0.842 m respectively. The value for root mean squared error is close to that obtained for comparisons of ERS-2 and Envisat satellite altimetry to in-situ water elevation data in similar basins (0.79 m and 0.47 m respectively). The model results imply that the bimodal annual pattern of Congo river discharge is predominantly a hydrological rather than hydraulically-controlled feature, with the channel-floodplain interactions and river constrictions having only a modest impact on the flood wave propagation. Nevertheless, and counter to current understanding, we find that interactions between channels and floodplains do however occur extensively, with over 2100 kilometres of the 13,000 kilometres of channel network in the model identified as zones where water is actively exchanged between channels and floodplains. Whilst the water volume that is exchanged with the floodplain is substantially less than for other large rivers, our results imply that channel-floodplain interactions are a significant feature of Congo flood wave propagation. Overall the model provides insights into the hydraulics of this understudied system that can next be tested both in the field and through more detailed modelling studies.

1 Introduction:

The Congo is the world's second largest river in terms of catchment area (3,687,000 kilometres^2) and annual average discharge (41,800 m^3 s^{-1}), and for the basin's population it provides a lifeline that accounts for the nearly three-quarters of all transportation routes in the region (Ladel et al., 2008). The Congo Basin also contains the world's second largest area of tropical forest (2 million km^2, Laporte et al., 1998), the majority of which is located in the Cuvette Centrale wetlands in the centre of the basin. Wetlands play an important role in many parts of the Earth system, with major impacts on global climate, water supply, biodiversity and food supply (Naiman et al., 1998). In particular, wetlands in tropical and sub-tropical regions are important sources of methane, possibly accounting for up to 75% of total global emissions from wetlands to the atmosphere (Matthews, 2000).

Despite this, the Congo Basin (Figure 1) is the least studied of the world's largest rivers (Alsdorf et al., 2016). Moreover, of the published works on the Congo, almost none have examined the hydraulic behaviour of the river. Most studies that have focused on water in the Congo Basin have instead investigated: (i) the climate of the region (Bultot and Dupriez, 1987; Labat et al., 2005; Laraque et al., 2001; Mahé et al., 2012); (ii) the hydrology and hydrological modelling of the Basin (Beighley et al., 2011; Tshimanga and Hughes, 2012; Tshimanga and Hughes, 2014); (iii) observation of wetlands through remote sensing (Betbeder et al., 2014; Bwangoy et al., 2010; Jung et al., 2010; Lee et al., 2014); (iv) the biogeochemistry of river, lakes and waterways (Laraque et al., 2013; Spencer et al., 2012) or (v) water level changes (Becker et al., 2014; Rosenqvist and Birkett, 2002). For a detailed review of the available literature and the Congo Basin in general, please see Alsdorf et al., (2016). With the exception of O'Loughlin et al. (2013), the river's hydraulic behaviour has been predominately investigated in relation to other research areas such as fisheries and fauna (Balon and Stewart, 1983; Colyn et al., 1991) or with regard to the formation of the basin over geological time (Crosby et al., 2010). Yet, hydraulic processes, such as downstream propagation of the flood wave and its interaction with floodplain wetlands, are of fundamental scientific importance and a strong

control on ecology, biogeochemistry and sediment transport within the basin. Flood wave dynamics also strongly affect navigation, water resources and power generation for the basin's population.

In this paper we seek to test two hypotheses regarding Congo flood wave dynamics. First, we seek to better understand whether hillslope rainfall-runoff or channel and floodplain processes, i.e. interactions between river channels and floodplains, are the more dominant control on the development of the Congo's bimodal flood pulse. This feature is unique amongst large river system but what causes it is still quite poorly understood. A working hypothesis (see for example, Figure 4 in Alsdorf et al., 2016) is that the tropical rainbelt which migrates from South to North across the basin from December to October produces flood pulses in both the main stem and tributaries which then either synchronise or desynchronise according to the different length of the flow pathways and varying wave travel times in the sub-basins. This pattern of tributary wave synchronization/desynchronization with the main stem flood pulse then creates the bimodal hydrograph observed at downstream gauging stations. However, it is unclear whether the timing of hydrological inputs to the main stem and tributaries is either more or less important to the creation of this feature than in-channel and floodplain process which affect the speed at which flood waves propagate once they have been generated. Key in-channel process which could potentially affect whether main stem and tributary flood waves either synchronise or desynchronise include: (i) evaporation from rivers, lakes and floodplain open water; (ii) the presence of river channel constrictions (e.g. O'Loughlin et al., 2013); and (iii) channel-floodplain interactions. Second, recent satellite observations by Lee et al (2011) have led to the hypothesis (Alsdorf et al., 2016) that the main source of water in the wetlands of the central Congo basin, the so-called Cuvette Centrale, is terrae-firma runoff and not the fluvial process of river-floodplain water exchange as in the Amazon.

Because in-situ river gauging data to properly test these hypotheses are lacking, an alternative method is to simulate water level and discharge dynamics with a high quality and suitably calibrated hydraulic model. Experimentation with such a model then allows the importance to wave

propagation of above three factors (evaporation, constrictions and channel-floodplain interactions) to be rigorously tested. Previous studies using a similar approach but answering different science questions have been described by Wilson et al (2007) who simulated floodplain inundation in the 30,000km^2 confluence plain lying between the Solimões and Purus rivers in the central Amazon basin, Biancamaria et al (2011) who simulated inundation over a 1000km reach of the Ob river in Siberia and Neal et al (2012) who simulated the impact of floodplain channels on the inundation dynamics of the inner Niger Delta in Mali. Such methods therefore have a rich heritage., and hence this is the approach adopted here where we present the results from a hydraulic model built for the entire ~1600 km length of the middle reach of the Congo and its six main tributaries. This model is driven by a mixture of in-situ discharges and runoff outputs from the Hillslope River Routing (HRR) hydrological model (Beighley et al., 2011) and is calibrated using satellite radar altimeter measurements of channel water surface height. This model uses the newly created, open-source, vegetation corrected SRTM digital terrain model, BEST (O'Loughlin et al., 2016). We use this model to test the above hypotheses and thereby improve our understanding of the hydraulics of the Congo Basin and the influence of the floodplain on the overall system.

2 Methodology:

A schematic diagram of the full procedure, described in more detailed below, is shown in Figure 2.

2.1 Study Area

The source of the Congo River lies in the southeast of the Democratic Republic of the Congo at an altitude of between 1400 and 1500 m, and consists of a number of small streams, swamps and lakes (Runge, 2008). The Congo River is often divided into three sections. The upper reach, known as the Lualaba, covers the 2,600 kilometre reach from the headwaters of the basin to the Boyoma Falls, just upstream of Kisangani. The middle reach flows for approximately 1600 kilometres between the Boyoma Falls to Malebo Pool, just upstream of Kinshasa, and the lower reach covers the ~500

kilometres from Malebo Pool to the Atlantic Ocean. The middle reach is very different in character from the upper and lower reaches, with water surface slopes averaging around 5.5 cm/kilometres (O'Loughlin et al., 2013), whereas the average slopes for the lower and upper reaches are ~60 cm/kilometres and 38 cm/kilometres respectively.

A number of large tributaries discharge into the middle reach, including the Oubangui, Mongala and Sangha which drain highlands north of the main stem and the Kasai, Lulonga and Lomami which flow from the south. The Congo River at Kinshasa has a bimodal discharge pattern, with a small peak around April - May and a large peak around November – December (see Figure 4 in Alsdorf et al., 2016). It is hypothesised that this is due to the arrangement of these tributary basins and their confluences with respect to the movement of the tropical rainbelt over the basin. Moreover, there is only a (relatively) small difference in high and low flow, with a ratio of 2.8 between the annual maximum and minimum average discharges (Runge, 2008).

This study focuses on the central portion of the Congo Basin (3) between 4.8^{o} N and 7.7^{o} S and 15.12^{o} E and 25.26^{o} E. This region includes the entire middle reach of the Congo River, and the major tributaries on the northern and southern banks. The total area covered by the model is 1.6 million km^2 or 44 % of the entire basin and includes the entire Cuvette Centrale wetland. Over 13,000 kilometres of river channel are modelled, of which most are navigable.

2.2 Digital Elevation Model

In hydraulic modelling, the DEM is one of the most critical inputs (Sanders, 2007). In data-sparse areas space based DEMs are invaluable, with the Shuttle Radar Topography Mission (SRTM) being the most popular. However, all space-based DEMs suffer, among other things, from significant vegetation biases that must be accounted for in order to avoid forested areas appearing as elevated land on floodplains. In this study, we use a newly created 3 arc-second vegetation-corrected SRTM dataset from O'Loughlin et al. (2016) to build the hydraulic model. This dataset (called BEST) is freely

142 available from http://data.bris.ac.uk/data/dataset/10tv0p32gizt01nh9edcjzd6wa. At 3 arc-second
143 resolution this DEM has a root mean square error in ground elevation for vegetated areas in Africa
144 of 4.75 m compared to 12.62 m for the void-filled version 4 SRTM DEM (Jarvis et al., 2008). It was
145 developed by applying an empirical elevation correction based on climate regions and vegetation
146 heights from the Vegetation Continuous Field data of DiMiceli et al. (2011). We applied a 2-D
147 adaptive smoothing algorithm to this dataset followed by a median filter, as suggested by O'Loughlin
148 et al. (2016), to remove noise and small artefacts. This filtered DEM was then resampled from 3-arc-
149 seconds to four kilometres which reduces the ground elevation Root Mean Squared Error to 0.12 m.

150 ## 2.3 Hydrodynamic model

151 We utilise a recent re-formulation of the LISFLOOD-FP model (Figure 4) (Neal et al., 2012) which
152 solves the shallow water equations omitting only the convective acceleration term (Bates et al.,
153 2010) over a structured grid using an explicit finite difference scheme to produce a two-dimensional
154 simulation of floodplain hydrodynamics. The model time step is determined using the Courant-
155 Friedrichs-Lewy condition. The numerical scheme is very well behaved (see de Almeida et al ., 2012)
156 and no stability or mass conservation issues were noted in any of the model simulations. LISFLOOD-
157 FP uses a sub-grid representation of river channels and was designed for areas, such as the Congo,
158 where little or no channel information is available. Channels are thus represented as 1D sub-grid
159 scale features and their width can be greater or smaller than the overlying floodplain grid. The
160 introduction of sub-grid channels requires additional parameters for channel widths, depths and
161 bank elevation. Of these, width and bank elevation can be derived from satellite imagery and digital
162 terrain data respectively, whilst river depth is treated as a free parameter and is calibrated along
163 with channel friction. Calibration was performed by minimising the fit between predicted water
164 surface elevations and observations of water surface height obtained from satellite radar altimetry
165 at 33 "virtual gauge" locations (described in detail below). When the channel water depth exceeds

the channel bank elevation mass is transferred to the overlying structured grid and the evolution of floodplain inundation in two-dimensions is simulated.

A four-kilometre spatial resolution hydrodynamic model was created for the study area described above, resulting in 98,350 cells. This spatial resolution was chosen as a compromise between computational cost (given the large number of simulations required to calibrate the model) and the ability of the model to adequately resolve details of floodplain inundation patterns. The chosen resolution corresponds to the average width (3.9 kilometres) of the Congo River between Kisangani and Kinshasa estimated by O'Loughlin et al (2015). However, because channels are represented as sub-grid scale features they are represented with their correct observed width. LISFLOOD-FP has previously been shown to reproduce accurate channel and floodplain water levels using similar resolution grids and sub-grid scale channels (Biancamaria et al., 2011; Neal et al., 2012; Wilson et al., 2007). As very little is known about the river morphology we assumed that all the channels are rectangular. Neal et al (2015) demonstrated that LISFLOOD-FP models with rectangular channels and calibrated channel friction had similar water level simulation accuracy to ones where channel shape was also allowed to vary. Given that we calibrate channel friction and depth in this study it is therefore unlikely that the channel shape assumption will impact the model results. The channel depths obtained through calibration are piecewise constant around each altimetry virtual station. This enables us to estimate spatially varying river depths throughout our study region.

The cell elevations (floodplain elevation) and bank elevations were obtained from the BEST terrain data set (O'Loughlin et al., 2016). Cell elevations are used for the routing of water across the floodplain, while the bank elevations are only used in the estimation of the channel depths. Channel widths every 250 m for the middle reach of the Congo were previously calculated by O'Loughlin et al., (2013) using Landsat imagery, and we have applied the same methodology to the entire area studied here. The sub-grid channel width in each 4 kilometre model cell is the average of the 250 m channel width data that it contains. These values correspond well with the study by O'Loughlin et al.

(2013) that found the channel width of the Congo varied from 500 m at Boyoma Falls to over 10 kilometres just upstream of Kinshasa at Malebo Pool. O'Loughlin et al. (2013) also noted that a number of significant constrictions occurred along the middle reach that created significant backwater effects that affected the water surface slope for tens to hundreds of kilometres upstream.

2.4 Model boundary conditions and discharge Data

Model boundary conditions at all upstream inflow points consisted of daily discharge obtained from in-situ observations or daily discharge outputs from the HRR rainfall-runoff model (both described in detail below), whilst at the downstream outlet a stage boundary condition based on daily observations at the Kinshasa gauge was imposed.

2.4.1 In-situ Discharge

As mentioned previously, there is a shortage of recent in-situ measurements of discharge in the Congo Basin. The Global Runoff Database (GRDC) has 96 station records of discharge across the entire Congo Basin, but of these only 21 have any data since 2000. For our study area, there are even fewer, with only three GRDC gauges available. However, data for three further in-situ gauges were obtained from the International Commission of the Congo-Oubangui-Sangha Basin (CICOS), and discharge estimates for additional basins were obtained from the Hillslope River Routing (HRR) hydrological model (Beighley et al., 2011; Lee et al., 2011).

To minimize the number of missing days in the in-situ observations the period from January 2000 to December 2003 was chosen for model simulations. As there are so few discharge records for the Congo region, the errors or uncertainties associated with these data are not well characterized, and generic estimates of discharge uncertainty can vary greatly. Di Baldassarre and Montanari (2009) estimate a 5% uncertainty in discharge measurements in ideal situations, and higher values in

more typical cases. Clarke et al. (2000) looked at uncertainties in mean discharges for the Parana and Amazon and found 4% and 16% uncertainties in the annual mean flows respectively. From anecdotal evidence, the error in the rating curve used at Kinshasa is approximately 5%; however, this seems somewhat optimistic and a 10% uncertainty bound may be a more conservative estimate.

Figure 5 shows the flow records for the in-situ measurements used. Only two of the three gauges from the GRDC were used (the Congo main stem at Kinshasa and the Oubangui at Bangui) as the third (the Congo main stem at Brazzaville) is for the same section as Kinshasa but has a shorter record. These records were nearly complete for the period of interest, with no missing records for Kinshasa and only 10 missing days in May-June 2001 at Bangui. These missing values were infilled by fitting third-order polynomials to the existing data. The stage data for Kinshasa was used as the model downstream boundary, whilst the data from the Bangui gauge provided the inflow discharge for the Oubangui tributary.

The three remaining observation records were obtained from CICOS. These records consisted of water-level measurements and corresponding rating curves for Ouesso on the Sangha River, Lediba on the Kasai River and Kisangani which provides the upstream boundary on the Congo main stem. Of these records, Ouesso on the Sangha River had no missing data during the study period. The gauge at Lediba on the Kasai River had 24 days of missing data, consisting of three very short periods less than two days and one period of ten days in May-June 2002. Missing data for Lediba was similarly infilled by fitting third-order polynomials to the existing data. However, the gauge at Kisangani was missing 1070 days out of 1461 (~73%) between January 2001 and December 2003. This large period of missing data was filled in using a combination of nearby Envisat observations of water level and the long-term discharge pattern. Two satellite altimetry virtual gauging locations, each with overpass frequencies of approximately 35 days, pass within 25 kilometres of the gauging location at Kisangani. The long-term datasets of surface water height at these virtual gauging locations were highly correlated with the Kisangani gauge (R^2 equal to 0.9 and

0.88 respectively). These two locations provided 41 data-points which in conjunction with the long-term historical discharge pattern was used to estimate flows during the periods of missing data at Kisangani.

2.4.2 Modelled Discharge

Inflows from the four in-situ gauges used to set the upstream boundary conditions for the model (Kisangani on the Congo, Ouesso on the Sangha, Bangui on the Oubangui and Lediba on the Kasai) account for only 57.7% of the total discharge at Kinshasa over the study period. With no other contemporary in-situ measurements available for the entire of the Central Basin it was necessary to utilise another source of discharge data for the remaining ungauged tributaries, and the obvious solution here is to use the outputs from a basin scale hydrological model driven with observed rainfall for the study period. There are a few hydrological models built for the Congo Basin, including the PITMAN-GW model (Tshimanga and Hughes, 2012), however only the HRR model (Beighley et al., 2011) is run at a daily time-step. While discharge outputs from a hydrological model with a monthly time-step could have been used, it was determined that a daily time-step would better capture the system dynamics, especially in smaller basins.

The HRR model operates on irregular model units (i.e. catchments) defined by topographic boundaries and the corresponding river network (Beighley et al., 2009). For each catchment, the landscape is approximated as an open book with two planes (i.e. hillslopes) draining laterally to a main river channel. Flow routing is performed using variants of the kinematic wave method for lateral surface and subsurface runoff, and diffusion wave methodologies (i.e. Muskingum-Cunge) for river discharge. Rainfall is separated into surface runoff and infiltration using the Green-Ampt method and subsurface runoff is generated using vertical Darcy flow methods. Runoff generation and routing processes are controled by three parameters each (i.e. six key parameters in total),

262 which were calibrated with available streamflow measurements (Beighley et al., 2015; Seyyedi et al.,
263 2015).

264 The HRR model was forced using the TRMM (3B42) precipitation datasets and calibrated using
265 satellite observations of river stage and then used to simulate the temporal pattern of river flow.
266 However, as HRR was not calibrated with a large spatially extensive flow record errors for discharge
267 prediction can be large. Comparing HRR predicted discharge to available flow observations in the
268 basin shows that it over-estimates the discharge for the upper Congo at Kisangani by a factor of 2,
269 the discharge of the Ubangui River at Bangui by 1.5 and under-estimates the discharge on the Kasai
270 River at Lediba.

271 To address this issue the discharge from the HRR model was compared to historical discharge
272 data for nine gauges across the study area for periods in the 1970s and 1980s to derive a simple
273 relationship (R^2 = 0.84) between the ratio of discharge to precipitation and the slope of the longest
274 flow path of each catchment. This relationship was then used to bias-correct the discharge outputs
275 from the HRR model for nineteen locations across the study area, corresponding to largest
276 tributaries draining directly into the Congo River. Of these, for the twelve largest basins time-varying
277 outputs were taken from the HRR model and used as an input to LISFLOOD-FP, whilst in the seven
278 locations with smaller upstream catchment areas a constant average discharge was used. The
279 locations of the constant discharges correspond to confluences in the river network and the
280 contributing areas and discharge are relatively small (~6%) compared to the observed discharge at
281 Kinshasa. Therefore, the use of constant rather than time varying discharges for these small
282 catchments should not have a significant impact on the overall results. The discharge outputs taken
283 from the HRR model account for approximately 38 % of the discharge at Kinshasa. When the in-situ,
284 modelled and constant discharges are combined, they account for 95.7% of Kinshasa's observed
285 (Figure 3(A)) discharge and are therefore within the likely error in discharge measurement at this
286 site.

2.5 Model simulations and calibration

Four different model setups were used in this study to help understand the flood wave dynamics of the Congo Basin and to assess how important certain processes (evaporation, channel-floodplain interactions, constrictions in river width) are to the development of the bimodal flood pulse. The simulation period was three years from between January 2000 to the end of December 2003, corresponding to the period with the largest amount of in-situ measurements available. Table 1 gives an overview of the four simulations that were run, including which model components were included in each simulation. Simulation 1, the control simulation, represents our current best view of the behaviour of the channel-floodplain system. It accounts for the spatial variability in river widths, allows for interaction between the river channels and floodplain (i.e. the exchange of water between river channels and surrounding floodplains), and includes evaporation (for all surface water) obtained from the CRU dataset (Harris et al., 2014). The impact of precipitation and infiltration on wave propagation was not tested as these processes are already accounted for by the HRR model that is used to set some of the hydraulic model boundary conditions. Open water evaporation, however, is not simulated by the hydrological model.

Channel depths and the channel friction parameter in the control simulation were calibrated using satellite altimetry observations of water level for 33 virtual gauging locations (Figure 3 (B)). Altimetry data were obtained from two different sources: 1) the ESA River and Lake Database (available from: http://tethys.eaprs.cse.dmu.ac.uk/RiverLake), who provide ERS-2 altimetry data; and 2) the database maintained by Laboratoire d'Etudes en Géophysique et Océanographier Spatiales (LEGOS), who provide Envisat data. Data for 16 locations were obtained from the former source, whilst Envisat data for the other 17 locations were obtained from LEGOS. The supplied ERS-2 data were referenced to the EGM96 vertical datum, whilst the Envisat data used EGM2008. The Envisat data were therefore converted to EGM96 to be consistent with the DEM used in this study and the ERS-2 altimetry. Da Silva et al. (2010), investigated the accuracy for both ERS-2 and Envisat for the Amazon

312 and found average root mean square errors of 0.792 m for ERS-2 and 0.47 m for Envisat, both errors
313 with a standard deviation of 0.366 metres. Whilst Envisat data has previously been used to better
314 understand the hydrology of the Congo river system (Lee et al., 2011; Becker et al., 2014),
315 comparable satellite altimetry validation studies to Da Silva et al. (2010) have not been carried out
316 because the Congo in-situ observations of water level have not yet been referenced to a common
317 geoid. However, given the similar width of the Amazon and Congo the accuracy of radar data
318 processing should be broadly equivalent and theoretically we should expect similar errors. In the
319 absence of any evidence to the contrary we therefore assume that the error values of Da Silva et al.
320 (2010) derived for the Amazon basin also apply in this study.

321 To perform the calibration the river channels in the model were divided into thirty-three
322 piecewise linear segments, based on the number of individual virtual gauges with each segment
323 centred on a virtual gauge. During calibration, a constant channel depth, assuming a rectangular
324 channel, for each region and a global Manning's n friction value for all 13,000 line kilometres of river
325 channel in the model domain were optimised. River widths, as previously mentioned, were obtained
326 from Landsat Imagery. The Manning's n friction coefficient for the floodplain was not calibrated and
327 was simply set to a spatially constant value of 0.1, assuming medium to dense brush (Chow, 1959)
328 because preliminary runs showed the model to not be sensitive to this parameter. Calibration was
329 undertaken using the fminsearch (Unconstrained nonlinear minimization) solver in MATLAB's
330 optimisation toolbox which uses the simplex search method of Lagarias et al. (1998). This was used
331 to minimise the sum of the root mean square errors between modelled and observed water heights
332 at each virtual gauge and ensured each virtual gauge was assigned the same weight no matter the
333 number of altimetry observations. The method therefore results in a global optimum rather a
334 solution that guarantees a locally optimal result at each virtual gauge.

335 Calibration was performed across 48 threads of a 10-core 2.3 GHz Intel Xeon E5-2650 v3
336 processor over a six-week period and in excess of 6000 simulations were required. Hydraulic model

computational cost increases by an order of magnitude with each halving of grid resolution so this explains the choice of a 4km resolution for the model. Even reducing the grid resolution to 2 km would increase the calibration compute time to more than a year, even on such a powerful machine After calibration, the optimised channel depths (average depth = 10.93 m) and global channel friction value (Manning's n = 0.0436) were varied one-at-a-time to ensure the optimal parameters where found. The average volume error for the calibrated simulation was $4x10^{-7}$ m^3.

The remaining simulations, (2, 3 and 4) used the calibrated depths and friction values from the control simulation, Simulation 1, to test the importance of: evaporation processes (Simulation 2); channel-floodplain interactions (Simulation 3) and; constrictions in river widths (Simulation 4). For Simulation 2, the evaporation component of LISFLOOD-FP was deactivated. In Simulation 3, the floodplain elevation was increased to prevent interactions between channels and floodplains and for Simulation 4 the large constrictions in river width (defined here as where the width of a river narrows and expands by more than 1000 m within five pixels (20 kilometres)) were removed. To do this a five by five filter window was passed over the river widths and where a constriction was identified the width was changed to the average of the filter. The removal of large constrictions increased the river width in 34 out of 3251 cells containing a sub-grid river channel over the entire study area.

The spin up procedure was identical for each simulation. Due to the short period of in-situ measurements, the models were run twice: first the models were used to simulate the year 2000 and the results provided the initial starting conditions for a second run, which covered the entire period repeating the year 2000. The performance of the second run was assessed by investigating how well the simulated water levels match the virtual gauges using Root Mean Square Error (RMSE) and bias. At the downstream boundary at Kinshasa, the simulated discharges were compared to independent in-situ measurements obtained from Global Runoff Data Centre using the Nash-Sutcliffe Efficiency (NSE) and RMSE. These performance criteria were calculated from day 100 after

the start of the second simulation runs to ensure any errors caused by the initial starting conditions were negligible.

2.6 Assumptions, limitations and Uncertainties

In the previous sections, several assumptions, limitations and uncertainties were introduced, that will be summarised here. Due to the lack of available data, several assumptions were required to model the Congo Basin. It is assumed that river channels are rectangular, as there is little data available on the bathymetry of the Congo River and this is a reasonable starting position. Floodplain friction was not calibrated and was assigned a value *a priori*. This was done to simplify the model calibration but would not have impacted the results significantly because of the low floodplain velocity. Due to the lack of in-situ measurements of discharge, it was necessary to combine both in-situ and modelled discharges which may have introduced uncertainties into the study. The most critical component of any flood/inundation model is the accuracy of the DEM. In this study, we used a 3 arc-second vegetation-corrected SRTM dataset from O'Loughlin et al. (2016) which has a root mean square error of 0.12 m at the model grid resolution. Bathymetry and river channel friction were calibrated using virtual gauging station data obtained from the ERS-2 and Envisat radar altimetry satellites, which have corresponding vertical errors of 0.79 m and 0.47 m respectively. The impact of precipitation and infiltration errors on wave propagation was not investigated.

3 Results:

Simulated water levels, discharges, inundation extents and volumes are compared to observed datasets below.

3.1 Discharge comparison

The simulated flow hydrograph at Kinshasa was compared to the corresponding in-situ discharge obtained from the GRDC. The Kinshasa in-situ discharge record was not used in the calibration of the

385 control simulation and so is independent of the model, although the gauged water elevation is
386 necessarily used as a model boundary condition. Table 2 shows the Nash-Sutcliffe efficiency (NSE),
387 RMSE (m^3/s) and the percentage of missing volume at Kinshasa over the entire simulation period (1
388 January 2000 – 31 December 2003). Simulation 1, the control, provided the highest NSE score and
389 the lowest RMSE. Simulation 2, with no evaporation, had a slightly higher RMSE than the control and
390 a very slightly lower NSE (0.8373 compared to 0.8386). This difference is unlikely to be significant
391 given typical errors in gauged discharge. Simulation 4, without constrictions, was next with only
392 slightly worse NSE and RMSE. Simulation 3, with no floodplain interaction, only resulted in an NSE
393 0.049 lower than the control simulation and with an increase in RMSE of 2,133 m^3/s or ~5% of the
394 mean annual discharge.

395 Based on the mass-balance calculations presented earlier, approximately 4% of the
396 discharge at Kinshasa is missing from the model inflow boundary conditions. All simulations had
397 approximately this volume missing, with less than 1% variation between the simulations. This
398 variation is approximately equal to 400 m^3/s, an amount that is insignificant when compared to the
399 average discharge of 40,662 m^3/s and the likely error in gauged flow of ~10%.

400 Figure 6 shows the simulated and observed hydrographs for the entire study period. All
401 simulations match the dynamics of the system adequately, in the sense that they can re-create the
402 double peak behaviour and both the low flow periods. However, the timing of the peak flow for
403 Simulations 3 and 4, corresponding to simulations without floodplain interactions and constrictions,
404 occurs earlier than in Simulations 1 and 2, and the observed flow record. This suggests that
405 simulations 3 and 4 are not attenuating the flood wave sufficiently.

406 Simulations 1 and 2, which correspond to the control and no evaporation simulations
407 respectively, match the timing of the observed peaks better; however, these simulations differ from
408 one another in how they match the receding (falling) limbs of the hydrographs. The receding limbs of

Simulation 1, the control simulation, are much steeper than those of Simulation 2, which has no evaporation, and the control simulation matches better the observed data.

3.2 Water Surface Heights

Simulated water surface heights for the four simulations were compared to the virtual gauging levels obtained from satellite altimetry observations. Table 3 shows the average Root Mean Square Error, RMSE (m) and average bias (m) for the four simulations compared with the observed water levels at the virtual gauging stations. Unsurprisingly the control simulation produced the lowest RMSE (0.842 m), followed by the simulations where evaporation was excluded (simulation 2, 0.845 m), the channel widths were smoothed (simulation 4, 0.884 m) and where interactions between floodplains and channels were excluded (simulation 3, 2.023 m). The simulation with no evaporation outperforms all other simulations for average bias, but not significantly so. There is little difference in bias between the no evaporation simulation (-0.162 m) and the control simulation (-0.185 m), and there is a large increase in bias error between these two model runs and the smoothed width (-0.393 m) and no floodplain simulations (1.735 m).

When we investigated the spatial distribution of the errors (Figure 7), one virtual gauging, location 23, had errors double those of the next largest. Table 3 shows the results when this location was excluded. The errors for location 23 could not be reduced further in this study. There are a number of potential sources for this error, which are discussed below. If location 23 is excluded then the average RMSE is reduced by ~5 cm and the average bias is reduced by nearly 7 cm in each case.

Figure 7 shows the spatial variation in water levels across the study area for the four simulations (lines) and the observed water levels for the virtual gauging stations (open dots). From the plots, Simulation 3 produces the highest water levels. This was expected because no transfer of water from channels to floodplains is allowed in Simulation 3 and, as a result, channel water elevations are correspondingly higher. There is very little variation between the remaining three

simulations, which all produce similar water levels across the study area, except at locations 25, 26 and 27 where Simulation 4 produces lower water levels than the other simulations. There are also eight locations (1, 3, 9, 28, 29, 31, 32 and 33) where the simulated and observed water levels for all four simulations are nearly identical. All simulations match the observed water levels in terms of timing and magnitude across the domain, except at three locations (23, 25 and 28). Location 23 was mentioned previously, and here the simulated water levels have the correct dynamic range but there is a bias. At this location three of the simulations (Simulations 1, 2 and 4) underestimate water level, whilst simulation 3 results in over-estimation. All simulations at location 25, except Simulation 3, reproduce the peak water level to within 0.5 m of the observed peak, but are unable to match the low flows. At location 28, similar to location 25, the simulated and observed water levels match at high flows to within 0.35 m, except for Simulation 4, but are unable to continuously match the low flows. At location 28 the low flows are well simulated in year one and are close in year three, but too low in year two.

Figure 8 shows the RMSE and bias at each virtual gauge for the control simulation. However, it should be noted that Simulations 2 and 4 (not shown) do comparatively well, compared with the control simulation in representing the observed water levels, with 32 of 33 locations having a sub-metre bias. This error is on par with the known errors associated with the DEM used (RMSE = 0.12 m) and the satellite altimetry virtual stations (whose RMSEs were estimated to be between 0.792 m and 0.47 m for ERS-2 and Envisat observations respectively). Location 23 is the exception with a 2.29 metre bias; however, the RMSE for this location is only 2.369 m, indicating that the size of this error is largely due to the bias. One potential reason for this large bias is that the virtual gauge data were obtained from ERS-2 observations. Da Silva et al. (2010) show that whilst average error for ERS-2 in the Amazon was 0.792 m with a standard deviation of 0.33 m, some individual sites showed deviations greater than 2 m. Alternatively, this bias may be due to errors in the DEM in the vicinity of location 23, resulting perhaps from an over-estimation of the amount of vegetation to be removed

458 from the original SRTM dataset. Only eight of the 33 locations have an RMSE greater than one
459 metre. At five of these locations (12, 13, 20, 23 and 25), the larger than average RMSE can be
460 explained by a corresponding similar size bias error. Of this subset of virtual gauging locations all
461 were obtained from ERS-2 observations apart from location 20. This could be a potential source of
462 the larger errors here. The three remaining locations (28, 30 and 31) have a relatively low bias
463 compared to the RMSE. These three locations correspond to sites on main tributaries, with location
464 28 on the Kasai, location 30 on the Sangha and location 31 on the Oubangui. These three locations
465 (28, 30, 31) are all ERS-2 virtual gauging stations. The errors at these locations could be due to
466 erroneous observations, particularly given these are smaller rivers so altimetry is less easy to
467 conduct.

468 ### 3.3 Identifying Active Floodplain Units

469 A unique result from the study was the identification of discrete regions where inundation occurs,
470 referred to as active floodplain units from here on. These active floodplain units were identified by
471 comparing the simulated water levels from Simulation 1 and 3 at the virtual gauging locations.
472 Where both simulated water levels are near identical, this indicates that only very limited channel-
473 floodplain interaction is occurring at these points. However, if the water levels for Simulation 3 are
474 significantly higher than the control simulation, this indicates that there are channel-floodplain
475 interactions affecting that location. The end of a unique active floodplain unit was deemed to be
476 where the simulated water levels returned to being approximately identical in the two simulations.
477 Four units were identified using this methodology. Three along the middle reach of the Congo
478 between points 1 and 3 (blue in figure 7); 3 and 9 (yellow), and 9 and 26 (purple). The final unit
479 occurs along the Sangha downstream of point 30 (green in figure 8) and joins the third unit along the
480 middle reach of the Congo. This analysis suggests that, to first-order, channel-floodplain interactions
481 occur along 2100 kilometres of channel and nearly the entire middle reach of the main stem.

3.4 Inundation Extents and Volumes

Figure 9 illustrates temporal variations in the simulated floodplain water volume and area. We utilise the inundation extent data set of Prigent et al. (2007) to compare to the simulated inundation extents. This dataset uses observations from multiple satellites to produce inundated fraction on a 0.25^{O} grid (~25 kilometres) for the corresponding time-period. Figure 9b, shows that simulations 1, 2 and 4 get the dynamics of the wetting and drying correct when compared to the Prigent et al. (2007) dataset. While they get both the timings correct and their averages are close to Prigent et al. (2007), their amplitudes do not match. However, the maximum difference is only 13% or 0.34% of the total pixels in the model domain. This difference is expected as the Prigent dataset is dataset is known to underestimate inundation when less than 10% of its grid cell is wet, overestimate inundation when 90% of a cell is wet or where a cell contains water-saturated soils (Aires et al., 2018). Simulation 3, which has no interaction between the channel and floodplain, has zero inundated area and is therefore not shown.

An issue in comparing the model output to data of Prigent et al (2007) is the large discrepancy between the ~25km resolution of the data and the 4km resolution of the model. To address this, Figure 10 shows the fractional inundated area at high and low water for the Prigent et al. (2007) data, for Simulation 1 at 4 km resolution and for Simulation 1 upscaled to the resolution of Prigent et al. (2007). Figure 10a and c show that Simulation 1 is able match the inundation extent along the main river channels but apparently over-estimates inundation along tributaries. However, this may also be because the coarse resolution of the data used to create the Pringent et al (2007) layer cannot pick up flooding in these narrower valleys. Figure 10a also highlights that the Prigent et al. (2007) data set is not able to identify inundation along certain reaches of the Congo, especially near the downstream boundary.

505 The intra-simulation comparison provides useful information on what controls the
506 inundation extent. The inundation extent in Simulation 4, where large constrictions were removed,
507 is approximately 1000 km^2 smaller than that of the control simulation (Simulation 1). The
508 comparison between Simulations 1 (control) and 2 (no evaporation) is more complex. In the wet
509 seasons, the maximum extents are virtually identical. However, the simulations diverge during the
510 dry seasons, with the control simulation inundation extent reducing more rapidly than Simulation 2
511 and having a smaller minimum extent as would be expected. Overall, the control simulation seems
512 to better match the wetting and drying process shown in the Prigent dataset (Prigent et al., 2007).

513 The patterns of floodplain volumes are similar to those found for inundation area with
514 Simulations 1 and 2 being near identical, while the floodplain volumes from Simulation 4 are on
515 average 5.9 km^3 lower than Simulation 1 (Control simulation). This was expected due to the
516 differences in floodplain extent and the impact of constrictions on backwater effects along the
517 Congo (O'Loughlin et al., 2013). However, unlike with floodplain extents, evaporation processes only
518 account for ~ 0.5 km^3 changes in floodplain volume. Lee et al. (2011) investigated Congo wetland
519 water volume changes using a combination of GRACE and satellite altimetry over an approximately
520 similar region to our model domain and estimated that the annual variation in floodplain storage to
521 be 111 km^3. The findings of this study suggest that the equivalent quantity in the model is on
522 average 90 km^3. Lee et al. (2011) also estimated the year-to-year variation in floodplain storage to
523 be 30 to 45 km^3, while this study estimates the annual variation to be 30.7 km^3.

524 **4 Discussion:**

525 The simulations show that floodplain interactions, evaporative processes and constrictions in river
526 width all affect the surface water dynamics of the Congo and its tributaries. While all four
527 simulations achieved Nash-Sutcliffe efficiencies greater than 0.75 at the downstream boundary at
528 Kinshasa, only Simulation 1 (the control) had been calibrated against satellite altimetry observations

of water level and the other three simulations used the same calibrated depths and global channel friction value (Manning's n = 0.03). Our simulations were also able to reproduce the water level dynamics (timing and vertical range) at the virtual gauges over the entire basin as well as water storage changes similar to those from GRACE (Lee et al., 2011). Our findings corroborate those of Neal et al. (2012) who found for the Niger inland delta that a hydrodynamic model calibrated spatially using ICESat satellite altimetry water levels can produce good downstream hydrographs.

In addition to satisfactory NSE scores, all simulations reproduced the bimodal hydrograph associated with the Congo Basin. This suggests that the bimodal hydrograph behaviour of the Congo River at Kinshasa is not due to channel and floodplain factors which affect the propagation of flood waves in the Congo main stem and major tributaries. Rather, the existing hypothesis (see for example Figure 4 in Alsdorf et al., 2016) that bimodality is due to meteorological (Becker et al., 2014) and hydrological factors is much more likely to be correct. Under this explanation the development of bimodality is principally due to: (1) the differential timing through the year of hydrological inputs from sub-catchments within the basin; and (2) the topology of the tributary network and main stem. The arrangement of tributaries and catchment shapes then controls how these separate flood peaks from the different sub-catchments either synchronize or de-synchronize when they arrive at the main stem, thus generating the bimodal behaviour observed at Kinshasa. According to our model simulations hydraulic controls play only a secondary role, and the impact of wave propagation along attenuating reaches between confluences (e.g. Turner-Gillespie et al., 2003) is not sufficient to change the synchronization or de-synchronization of these hydrologically generated peaks Hydraulics does however exert some influence as evidenced by the fact that Simulation 3 and Simulation 4, corresponding to no channel-floodplain interactions and no constrictions respectively, result in higher flood peaks and earlier times of peak flow at Kinshasa. This indicates that the interaction between the floodplain and the river channels and the constrictions in the width of the Congo and its tributaries exerts a modest influence on the overall propagation of the flood wave.

554 However, these effects are relatively small compared to that noted for other large rivers. Neal et al.
555 (2012) found that channel-floodplain interactions were essential to obtain accurate wave
556 propagation for the Niger inland delta, and similar results have been found for the Amazon (de Paiva
557 et al., 2013). Our finding that there are interactions between floodplains and channels also adds to
558 knowledge regarding the source of water in the wetlands of the central Congo basin. Previous work
559 (Lee et al., 2011) has suggested that Congo wetlands fill from terrae-firma runoff and not the fluvial
560 process of river-floodplain water exchange, however our work suggests that this is not wholly the
561 case and that a non-trivial contribution of river channel water also occurs.

562 While our simulations suggest that constrictions have only a modest effect on the wave
563 propagation at the downstream gauging station at Kinshasa, they have a more significant impact on
564 the inundation extents and floodplain volumes. Previous work by O'Loughlin et al., (2013)
565 highlighted that there are large constrictions in the width of the Congo along the middle reach and
566 these constrictions may result in large portions of the Congo being affected by backwater. In this
567 study, we find large constrictions result in an approximate 5% increase in the inundation extent and
568 a 10 % increase in the inundation volume.

569 Although the volume of water exchanged between the channel and floodplain in the Congo
570 is relatively small compared to other large unregulated rivers such as the Amazon, , these channel-
571 floodplain interactions occur extensively. Our results indicate that channel-floodplain interactions
572 occur for over 2000 kilometres of river channel in our model domain and along nearly the entire
573 middle reach of the Congo main stem. This finding contrasts with that of Lee et al., (2011), who
574 stated the floodplain wetland water levels were always greater than the river and therefore that
575 floodplains could not receive water from the river channels. Resolving the differences between
576 these contrasting pieces of evidence and determining the extent to which channels and floodplains
577 interact in the Congo basin should be a focus for future research in the region.

The results show that while evaporative processes have little effect on the propagation of the flood wave, in-channel water levels and floodplain storage, they have a more significant effect on the inundation extent. Simulations without evaporation (Simulation 2) produce near identical results to the control simulation for water-levels, the overall bimodal behaviour at Kinshasa and the inundation volumes.

Finally, interrogation of the model results can shed some light on the potential river depth and variations in stage across our study region (Figure 11). Alsdorf et al., (2016) based on previous publications (e.g. Runge, 2007; Marlier, 1973) estimated channel depths of between 'a few m' to more than 20 m just upstream of Kinshasa. This is consistent with the calibrated channel depths obtained in our modelling. Our maximum variations in stage from the control simulation (Simulation 1) are also consistent with previous studies, which estimated between two and three metres of stage variation along the middle reach of the Congo (Becker et al., 2014; Rosenqvist and Birkett, 2002; O'Loughlin et al., 2013; Lee et al, 2014) and larger variations in its tributaries (Becker et al., 2014).

5 Conclusions:

This paper has presented the results of the first large-scale hydraulic model for the Middle Reach of the Congo Basin and its tributaries. The model domain is 1,120 kilometres by 1,400 kilometres with a spatial resolution of four kilometres and contains approximately 13,000 kilometres of major river channels that are treated as sub-grid scale features. The domain also contains the Cuvette Centrale, one of the world's largest swamp forests. The hydraulic model is driven by a mixture of in-situ discharge and scaled hydrological model outputs. These inputs account for nearly 96% of the in-situ discharge at Kinshasa. The hydraulic model is calibrated by adjusting spatially varying channel depths

and a constant channel friction to maximize the fit to water level observations at 33 virtual gauging stations obtained from satellite radar altimetry observations.

The results show that a large-scale hydraulic model driven by a mixture of discharge sources can be calibrated to reproduce remotely sensed observations of water level in a data sparse basin with relatively small Root Mean Square (RMSE = 0.8417 m), small average bias (bias =-0.1853 m) and a high Nash-Sutcliffe Efficiency for discharge at the downstream gauge (NSE = 0.8386). The average model error in water level is close to the error in the altimetry observations themselves (0.79 m for ERS-2 and 0.47 m for Envisat), and the model can broadly reproduce the timing and dynamic range of channel water level variations across the basin at the virtual gauge locations. Using the calibrated parameters for the control simulation, three other simulations were run to investigate the impact of channel-floodplain interactions, evaporation processes and spatial variability of river widths.

The results highlight that both channel-floodplain interactions and constrictions in the river widths are needed to ensure that some aspects of the dynamics of the system are matched. While simulations without channel-floodplain interactions and without constrictions were able to produce high Nash-Sutcliffe Efficiency at the downstream boundary (NSE = 0.7897 and 0.8334 respectively), they resulted in poor attenuation of the flood wave and earlier times to peak than the observed discharge at Kinshasa. However, all simulations were able to produce the bimodal behaviour of the Congo at Kinshasa, indicating that the hydrology and network topology are primarily responsible for producing this behaviour.

Channel-floodplain interactions are widespread and occur over large parts of the domain. We estimate there are active interactions along 2100 kilometres of rivers within our study area, and along most of the middle reach of the Congo River itself. This contrasts with previous findings from remotely sensed data (Lee et al., 2011) that the wetlands of the central Congo basin fill from terrae firma runoff and not channel-floodplain interactions. This indicates that while channel-floodplain

interactions have only a modest impact on the bimodal discharge behaviour of the Congo at Kinshasa, they can be locally important for inundation extent and volume. Our results suggest that a mixture of local hydrology and floodplain-channel interactions are important to reproduce the storage changes estimated from GRACE.

Evaporative processes are also important for accurately simulating floodplain dewatering in the Congo Basin. While there was very little difference between the control simulation and Simulation 2 (with no evaporative processes included) across several evaluation criteria, including NSE at the Kinshasa gauge, RMSE of altimetry water levels and inundation volume, there was a noticeable difference in inundation extent. Both simulations, the control and Simulation 2, get the timing of the wetting and drying of the floodplain correct and have the same maximum and minimum extents. However, inundation extent in the control simulation reduces faster, matching the observed dewatering better than the simulation without evaporative processes.

From our control simulation, we can provide first-order estimates of both river depths and maximum variations in stage across the region. Our results are consistent with the finding of previous studies and show that: i) the Congo river, despite its large discharge, is relatively shallow and; ii) the maximum variation in stage is relatively small, with a maximum variation less than 7 m compared to a maximum variation in excess of 16 m in the Amazon (da Silva et al., 2012).

Overall the model simulations have given insights into the behaviour of river and floodplain flows within the Congo basin that could not be obtained using either remote sensing data or ground observations alone. However, the model represents only a first attempt, and further research is thus needed to investigate: the impact of floodplain channels; the role spatial resolution of the model may have and; the role of local hydrology on inundation extents and volumes. Nevertheless, the methods described could easily be applied in other river basins to elucidate controls on floodplain inundation in a wider variety of settings.

Acknowledgments:

Fiachra O'Loughlin was supported by The Leverhulme Trust grant RPG-409. J. Neal was supported by the DFID/Royal Society Africa Capacity Building Initiative. G. Schumann was supported by research funding from the National Aeronautics and Space Administration. E. Beighley was supported by NASA's GRACE Science Team (NNX12AJ95G) and Terrestrial Hydrology (NNX12AQ36G, NNX14AD82G) Programs. Paul Bates was supported by The Leverhulme Trust grant RPG-409, the DFID/Royal Society Africa Capacity Building Initiative, a Leverhulme Research Fellowship and a Royal Society Wolfson Research Merit award.

References:

Aires, F., Prigent, C., Fluet-Chouinard, E., Yamazaki, D., Papa, F. and Lehner, B., 2018. Comparison of visible and multi-satellite global inundation datasets at high-spatial resolution. Remote Sensing of Environment, 216, pp.427-441.

Alsdorf, D., Beighley, E., Laraque, A., Lee, H., Tshimanga, R., O'Loughlin, F., Mahé, G., Dinga, B., Moukandi, G., Spencer, R.G.M., 2016. Opportunities for hydrologic research in the Congo Basin. Rev. Geophys. 54, 2016RG000517. doi:10.1002/2016RG000517

Alsdorf, D.E., 2003. Water storage of the central Amazon floodplain measured with GIS and remote sensing imagery. Ann. Assoc. Am. Geogr. 93, 55–66.

Balon, E.K., Stewart, D.J., 1983. Fish assemblages in a river with unusual gradient (Luongo, Africa-Zaire system), reflections on river zonation, and description of another new species. Environ. Biol. Fishes 9, 225–252.

Bates, P.D., Horritt, M.S., Fewtrell, T.J., 2010. A simple inertial formulation of the shallow water equations for efficient two-dimensional flood inundation modelling. J. Hydrol. 387, 33–45.

671 Becker, M., da Silva, J.S., Calmant, S., Robinet, V., Linguet, L., Seyler, F., 2014. Water Level
672 Fluctuations in the Congo Basin Derived from ENVISAT Satellite Altimetry. Remote Sens. 6,
673 9340–9358. doi:10.3390/rs6109340

674 Beighley, R. E., Eggert, K., Wilson, C. j., Rowland, J. c., Lee, H., 2015. A hydrologic routing model
675 suitable for climate-scale simulations of arctic rivers: application to the Mackenzie River
676 Basin. Hydrol. Process. 29, 2751–2768. doi:10.1002/hyp.10398

677 Beighley, R.E., Eggert, K.G., Dunne, T., He, Y., Gummadi, V., Verdin, K.L., 2009. Simulating hydrologic
678 and hydraulic processes throughout the Amazon River Basin. Hydrol. Process. 23, 1221–
679 1235. doi:10.1002/hyp.7252

680 Beighley, R.E., Ray, R.L., He, Y., Lee, H., Schaller, L., Andreadis, K.M., Durand, M., Alsdorf, D.E., Shum,
681 C.K., 2011. Comparing satellite derived precipitation datasets using the Hillslope River
682 Routing (HRR) model in the Congo River Basin. Hydrol. Process. 25, 3216–3229.

683 Betbeder, J., Gond, V., Frappart, F., Baghdadi, N.N., Briant, G., Bartholomé, E., 2014. Mapping of
684 Central Africa Forested Wetlands Using Remote Sensing. IEEE J. Sel. Top. Appl. Earth Obs.
685 Remote Sens. 7, 531–542. doi:10.1109/JSTARS.2013.2269733

686 Biancamaria, S., Bates, P.D., Boone, A. and Mognard, N.M., 2009. Large-scale coupled hydrologic and
687 hydraulic modelling of the Ob river in Siberia. J. Hydrol. 379(1-2), 136-150.

688 Birkett, C.M., Mertes, L.A.K., Dunne, T., Costa, M.H., Jasinski, M.J., 2002. Surface water dynamics in
689 the Amazon Basin: Application of satellite radar altimetry. J. Geophys. Res. Atmospheres
690 1984–2012 107, LBA–26.

691 Bultot, F., Dupriez, G.L., 1987. Niveaux et débits du fleuve Zaïre à Kinshasa (régime-variabilité-
692 prévision). Koninklijke academie voor overzeese wetenschappen. Klasse voor technische
693 wetenschappen.

694 Bwangoy, J.-R.B., Hansen, M.C., Roy, D.P., Grandi, G.D., Justice, C.O., 2010. Wetland mapping in the
695 Congo Basin using optical and radar remotely sensed data and derived topographical indices.
696 Remote Sens. Environ. 114, 73–86. doi:10.1016/j.rse.2009.08.004

697 Clarke, R.T., Mendiondo, E.M., Brusa, L.C., 2000. Uncertainties in mean discharges from two large
698 South American rivers due to rating curve variability. Hydrol. Sci. J. 45, 221–236.
699 doi:10.1080/02626660009492321

700 Colyn, M., Gautier-Hion, A., Verheyen, W., 1991. A re-appraisal of palaeoenvironmental history in
701 Central Africa: evidence for a major fluvial refuge in the Zaire Basin. J. Biogeogr. 403–407.

702 Crosby, A.G., Fishwick, S., White, N., 2010. Structure and evolution of the intracratonic Congo Basin.
703 Geochem. Geophys. Geosystems 11.

704 da Silva, J., Calmant, S., Seyler, F., Lee, H., Shum, C., 2012. Mapping of the extreme stage variations
705 using ENVISAT altimetry in the Amazon basin rivers. Int. Water Technol. J. 2, 14–25.

706 da Silva, J., Calmant, S., Seyler, F., Rotunno Filho, O.C., Cochonneau, G., Mansur, W.J., 2010. Water
707 levels in the Amazon basin derived from the ERS 2 and ENVISAT radar altimetry missions.
708 Remote Sens. Environ. 114, 2160–2181. doi:10.1016/j.rse.2010.04.020

709 de Almeida, G., Bates, P.D., Souvignet, M. and Freer, J.E., 2012. Improving the stability of a simple
710 formulation of the shallow water equations for 2D flood modelling. Wat. Resour. Res., 48,
711 paper W05528. doi:10.1029/2011WR011570

712 de Paiva, R.C.D., Buarque, D.C., Collischonn, W., Bonnet, M.-P., Frappart, F., Calmant, S., Bulhões
713 Mendes, C.A., 2013. Large-scale hydrologic and hydrodynamic modeling of the Amazon River
714 basin. Water Resour. Res. 49, 1226–1243. doi:10.1002/wrcr.20067

715 Di Baldassarre, G., Montanari, A., 2009. Uncertainty in river discharge observations: a quantitative
716 analysis. Hydrol. Earth Syst. Sci. 13, 913.

717 DiMiceli, C.M., Carroll, M.L., Sohlberg, R.A., Huang, C., Hansen, M.C., Townshend, J.R.G., 2011.
718 Annual Global Automated MODIS Vegetation Continuous Fields (MOD44B) at 250 m Spatial
719 Resolution for Data Years Beginning Day 65, 2000–2010, Collection 5 Percent Tree Cover.
720 Univ. Md. Coll. Park.

721 Dunne, T., Mertes, L.A., Meade, R.H., Richey, J.E., Forsberg, B.R., 1998. Exchanges of sediment
722 between the flood plain and channel of the Amazon River in Brazil. Geol. Soc. Am. Bull. 110,
723 450–467.

724 Harris, I., Jones, P. d., Osborn, T. j., Lister, D. h., 2014. Updated high-resolution grids of monthly
725 climatic observations – the CRU TS3.10 Dataset. Int. J. Climatol. 34, 623–642.
726 doi:10.1002/joc.3711

727 Jarvis, A., Reuter, H.I., Nelson, A., Guevara, E., 2008. Hole-filled SRTM for the globe Version 4.
728 Available CGIAR-CSI SRTM 90m Database Httpsrtm Csi Cgiar Org.

729 Jung, H.C., Hamski, J., Durand, M., Alsdorf, D., Hossain, F., Lee, H., Hossain, A.K.M.A., Hasan, K., Khan,
730 A.S., Hoque, A.K.M.Z., 2010. Characterization of complex fluvial systems using remote
731 sensing of spatial and temporal water level variations in the Amazon, Congo, and
732 Brahmaputra Rivers. Earth Surf. Process. Landf. 35, 294–304. doi:10.1002/esp.1914

733 Labat, D., Ronchail, J., Guyot, J.L., 2005. Recent advances in wavelet analyses: Part 2—Amazon,
734 Parana, Orinoco and Congo discharges time scale variability. J. Hydrol. 314, 289–311.
735 doi:10.1016/j.jhydrol.2005.04.004

736 Ladel, J., NGUINDA, P., PANDI, A., KABOBO, C.T., TONDO, B.-L., SAMBO, G., TELLRO-WAI, N.,
737 BULUKU, A., 2008. Integrated Water Resources Management in the Congo basin based on
738 the development of Earth Observation monitoring systems in the framework of the AMESD
739 Programme in Central Africa. Presented at the 13th World Water Congress, September 1-4,
740 Montpellier, France.

741 Lagarias, J. C., Reeds, J.A., Wright, M.H. and Wright, P.E., 1998. Convergence properties of the
742 Nelder-Mead Simplex Method in low dimensions. SIAM Journal of Optimization. 9, 112–147.
743 doi: 10.1137/S1052623496303470

744 Laporte, N.T., Goetz, S.J., Justice, C.O., Heinicke, M., 1998. A new land cover map of central Africa
745 derived from multi-resolution, multi-temporal AVHRR data. Int. J. Remote Sens. 19, 3537–
746 3550.

747 Laraque, A., Castellanos, B., Steiger, J., Lòpez, J.L., Pandi, A., Rodriguez, M., Rosales, J., Adèle, G.,
748 Perez, J., Lagane, C., 2013. A comparison of the suspended and dissolved matter dynamics of
749 two large inter-tropical rivers draining into the Atlantic Ocean: the Congo and the Orinoco.
750 Hydrol. Process. 27, 2153–2170. doi:10.1002/hyp.9776

751 Laraque, A., Mahé, G., Orange, D., Marieu, B., 2001. Spatiotemporal variations in hydrological
752 regimes within Central Africa during the XXth century. J. Hydrol. 245, 104–117.

753 Lee, H., Beighley, R.E., Alsdorf, D., Jung, H.C., Shum, C.K., Duan, J., Guo, J., Yamazaki, D., Andreadis,
754 K., 2011. Characterization of terrestrial water dynamics in the Congo Basin using GRACE and
755 satellite radar altimetry. Remote Sens. Environ. 115, 3530–3538.

Lee, H., Jung, H.C., Yuan, T., Beighley, R.E., Duan, J., 2014. Controls of Terrestrial Water Storage Changes Over the Central Congo Basin Determined by Integrating PALSAR ScanSAR, Envisat Altimetry, and GRACE Data, in: Lakshmi, V., Alsdorf, D., Anderson, M., Biancamaria, S., Cosh, M., Entin, J., Huffman, G., Kustas, W., Oevelen, P. van, Painter, T., Parajka, J., Rodell, Matthew, Rüdiger, C. (Eds.), Remote Sensing of the Terrestrial Water Cycle. John Wiley & Sons, Inc, pp. 115–129.

Mahé, G., Rouché, N., Dieulin, C., Boyer, J.-F., Ibrahim, B., Crès, A., Servat, E., Valton, C., Paturel, J.-E., 2012. Carte des pluies annuelles en Afrique = Annual rainfall map of Africa.

Marlier, G., 1973. Limnology of the Congo and Amazon rivers. Trop. For. Ecosyst. Afr. S. Am. Comp. Rev. 223–238.

Matthews, E., 2000. Wetlands, in: Khalil, P.D.M.A.K. (Ed.), Atmospheric Methane. Springer Berlin Heidelberg, pp. 202–233.

Mertes, L.A., Dunne, T., Martinelli, L.A., 1996. Channel-floodplain geomorphology along the Solimões-Amazon river, Brazil. Geol. Soc. Am. Bull. 108, 1089–1107.

Naiman, R.J., Fetherston, K.L., McKay, S.J., Chen, J., 1998. Riparian forests. River Ecol. Manag. Lessons Pac. Coast. Ecoregion Springer-Verl. N. Y. 289–323.

Neal, J., Schumann, G., Bates, P., 2012. A subgrid channel model for simulating river hydraulics and floodplain inundation over large and data sparse areas. Water Resour. Res. 48.

Neal, J.C., Odoni, N.A., Trigg, M.A., Freer, J.E., Garcia-Pintado, J., Mason, D.C., Wood, M. and Bates, P.D. (2015). Efficient incorporation of channel cross-section geometry uncertainty into regional and global scale flood inundation models. J. Hydrol., 529 (1), 169–183. (10.1016/j.jhydrol.2015.07.026).

O'Loughlin, F., Trigg, M.A., Schumann, G.-P., Bates, P.D., 2013. Hydraulic characterization of the middle reach of the Congo River. Water Resour. Res. 49, 5059–5070.

O'Loughlin, F.E., Paiva, R.C.D., Durand, M., Alsdorf, D.E., Bates, P.D., 2016. A multi-sensor approach towards a global vegetation corrected SRTM DEM product. Remote Sens. Environ. 182, 49–59. doi:10.1016/j.rse.2016.04.018

O'Loughlin, F.E., Neal, J., Yamazaki, D. and Bates, P.D., 2016. ICESat-derived inland water surface spot heights. Water Resour. Res. 52(4), 3276-3284.

Prigent, C., Papa, F., Aires, F., Rossow, W.B., Matthews, E., 2007. Global inundation dynamics inferred from multiple satellite observations, 1993–2000. J. Geophys. Res. Atmospheres 112, D12107. doi:10.1029/2006JD007847

Rosenqvist, Å., Birkett, C., 2002. Evaluation of JERS-1 SAR mosaics for hydrological applications in the Congo river basin. Int. J. Remote Sens. 23, 1283–1302.

Runge, J., 2008. The Congo River, Central Africa. Large Rivers Geomorphol. Manag. Chichester John Wiley Sons Ltd 293–309.

Sanders, B.F., 2007. Evaluation of on-line DEMs for flood inundation modeling. Adv. Water Resour. 30, 1831–1843. doi:10.1016/j.advwatres.2007.02.005

Seyyedi, H., Anagnostou, E.N., Beighley, E., McCollum, J., 2015. Hydrologic evaluation of satellite and reanalysis precipitation datasets over a mid-latitude basin. Atmospheric Res. 164–165, 37–48. doi:10.1016/j.atmosres.2015.03.019

Spencer, R.G.M., Hernes, P.J., Aufdenkampe, A.K., Baker, A., Gulliver, P., Stubbins, A., Aiken, G.R., Dyda, R.Y., Butler, K.D., Mwamba, V.L., Mangangu, A.M., Wabakanghanzi, J.N., Six, J., 2012.

799 An initial investigation into the organic matter biogeochemistry of the Congo River.
800 Geochim. Cosmochim. Acta 84, 614–627. doi:10.1016/j.gca.2012.01.013

801 Te Chow, V., 1959. *Open channel hydraulics*. McGraw-Hill Book Company, Inc; New York.

802 Tshimanga, R.M., 2012. Hydrological uncertainty analysis and scenario based streamflow modelling
803 for the Congo River Basin. PhD thesis, Rhodes University repository. South Africa.

804 Tshimanga, R.M., Hughes, D.A., 2012. Climate change and impacts on the hydrology of the Congo
805 Basin: The case of the northern sub-basins of the Oubangui and Sangha Rivers. Phys. Chem.
806 Earth Parts ABC, 12th WaterNet/WARFSA/GWP-SA Symposium: Harnessing the rivers of
807 knowledge for socio-economic development, climate adaptation & environmental
808 sustainability 50–52, 72–83. doi:10.1016/j.pce.2012.08.002

809 Tshimanga, R.M., Hughes, D.A., 2014. Basin-scale performance of a semidistributed rainfall-runoff
810 model for hydrological predictions and water resources assessment of large rivers: The
811 Congo River, Water Resour. Res., 50,doi:10.1002/2013WR014310

812 Turner-Gillespie, D.F., Smith, J.A. and Bates, P.D., (2003). Attenuating reaches and the regional flood
813 response of an urbanising drainage basin. Advances in Water Resources, 26, 673 –684.
814 (10.1016/S0309-1708(03)00017-4).

815 Wilson, M., Bates, P., Alsdorf, D., Forsberg, B., Horritt, M., Melack, J., Frappart, F. and Famiglietti, J.,
816 2007. Modeling large-scale inundation of Amazonian seasonally flooded wetlands. Geophys.
817 Res. Lett., 34(15).

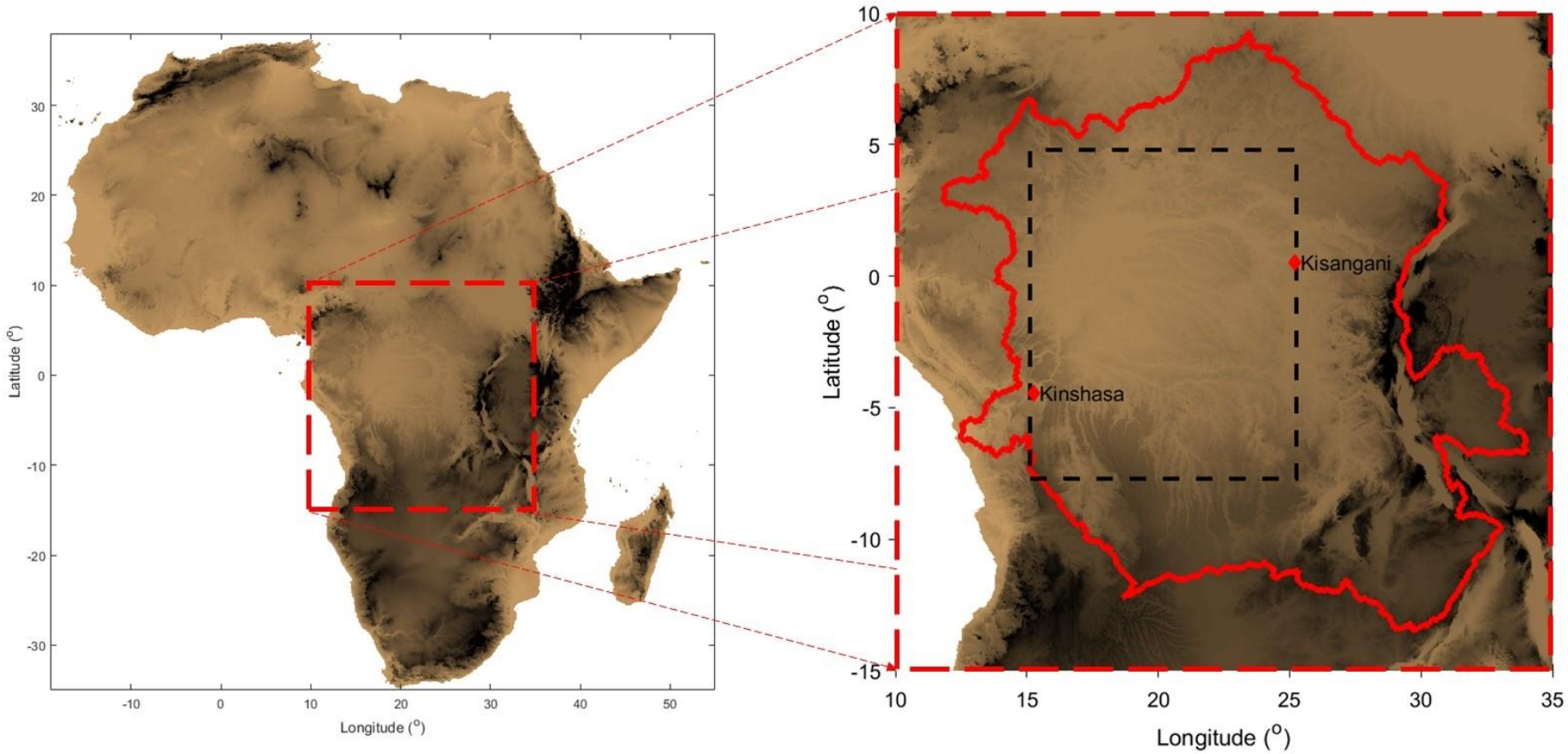

818

819 **Figure 1: Shaded relief map of Africa showing the outline of the Congo Basin (solid red) and the model domain that has been simulated (dashed black).**

820 **The red dots represent the locations of Kisangani and Kinshasa related to the model domain.**

821

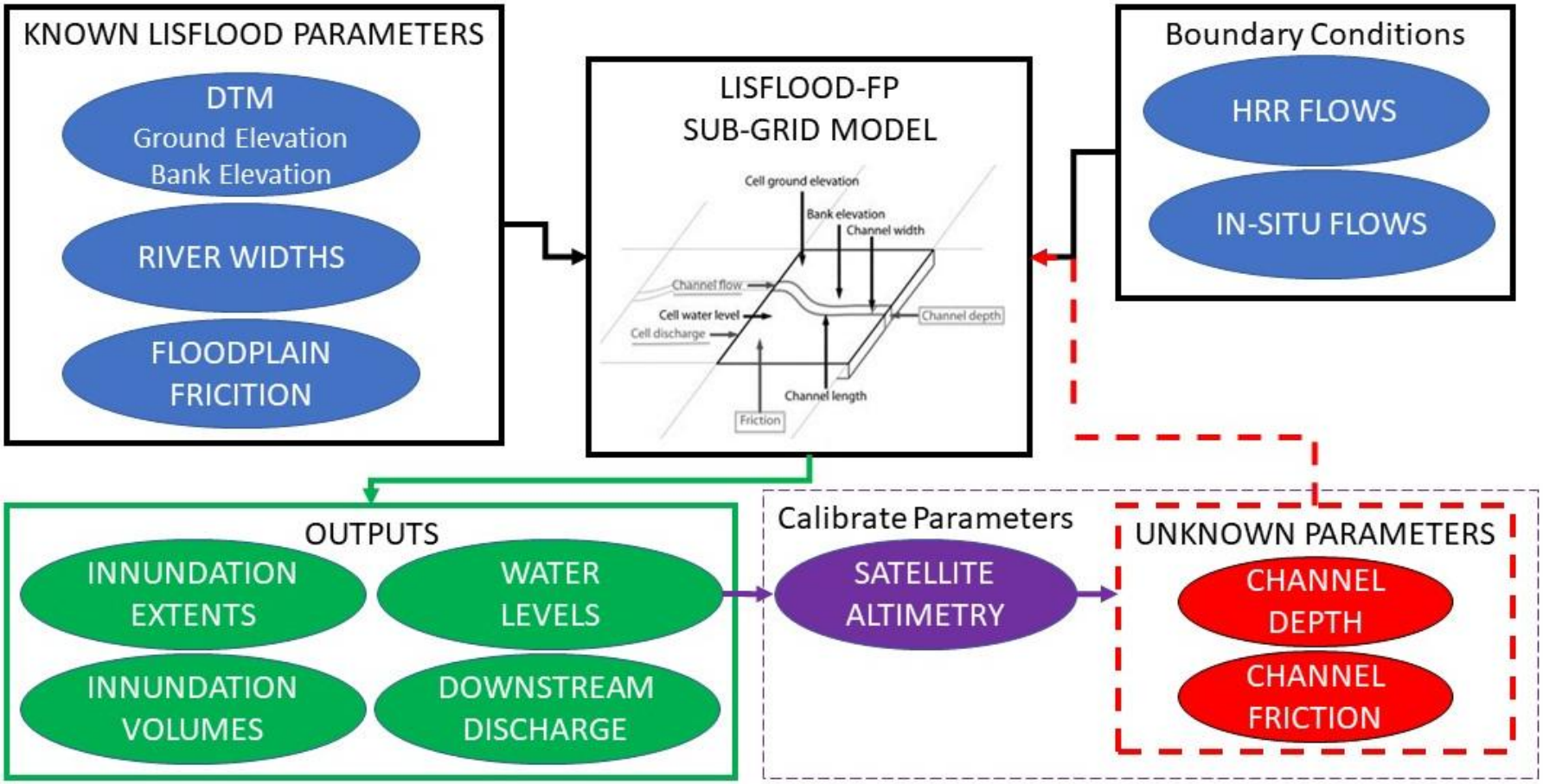

822

823 **Figure 2:Schematic of Methodology, showing known variables in blue, model output in green, unknown parameters in red and calibration procedure in purple, and how they relate to the**

824 **LISFLOOD-FP model.**

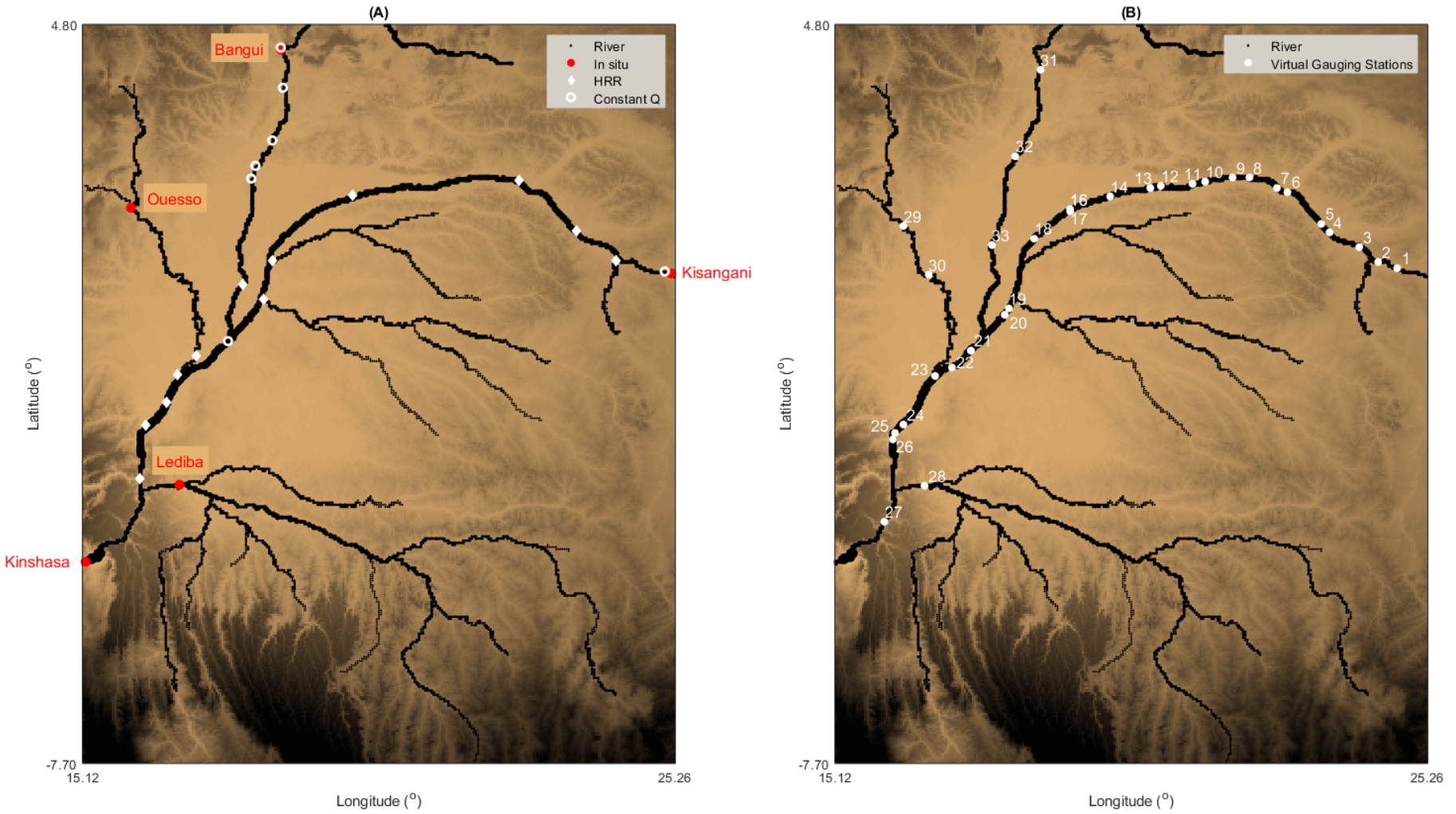

825

826 **Figure 3: Study Area showing rivers included in the hydrodynamic model and: (A) Location of discharge locations and source; and (B) ERS-2 and Envisat**

827 **Virtual Gauging Locations. Variation in river width ris epresented by weight of line.**

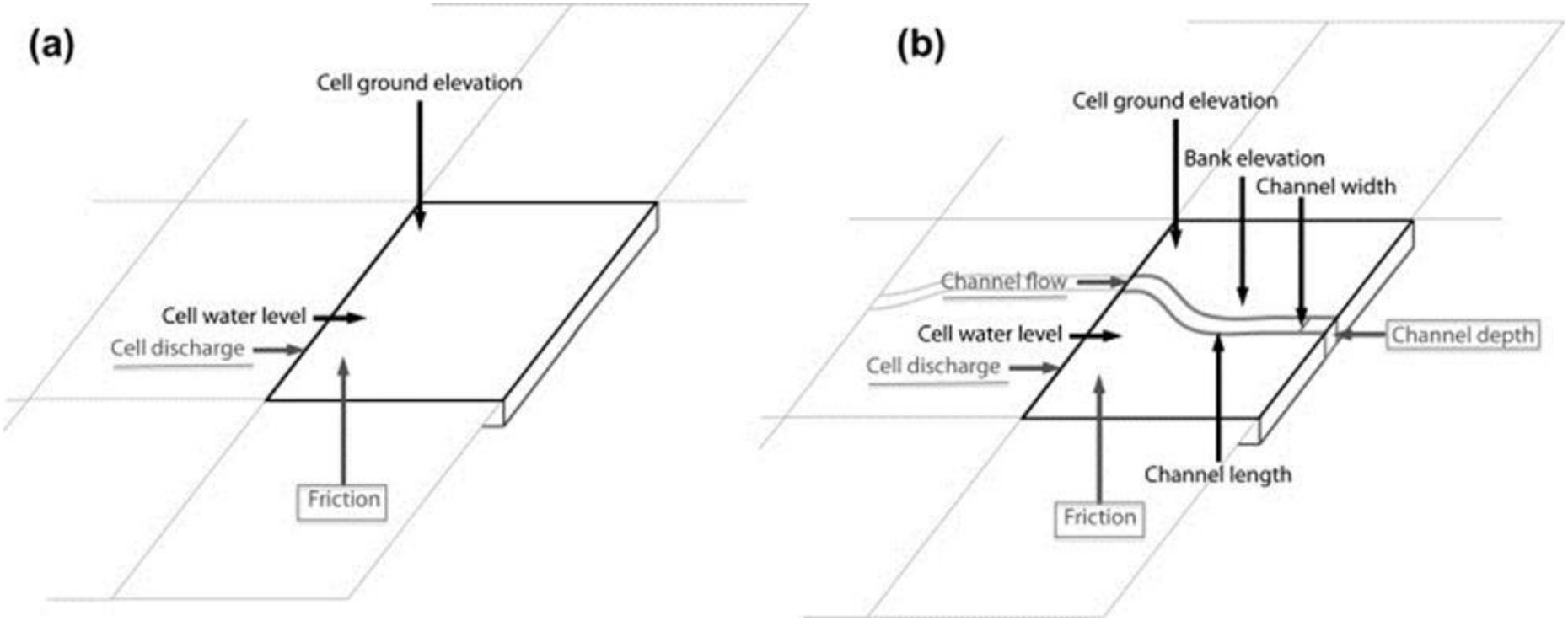

828

829 **Figure 4: Hydrodynamic model schematic of (a) a typical simple 2D raster based model and (b) the sub-grid channel routine as developed by Neal et al.**

830 **(2012).**

831

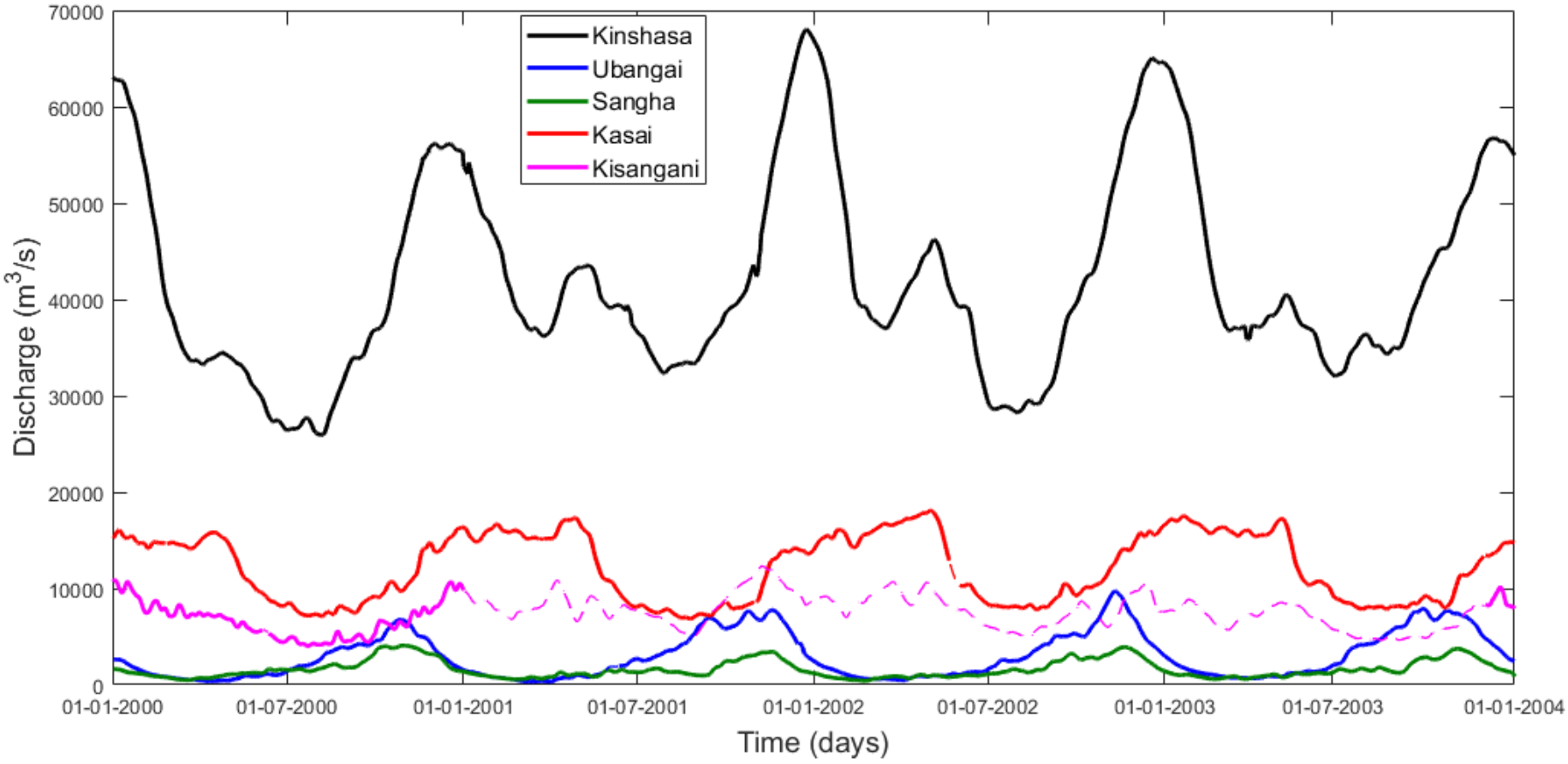

832

833 **Figure 5: Available in-situ observations of discharge. Missing data shown by a dashed-line (--)**

834

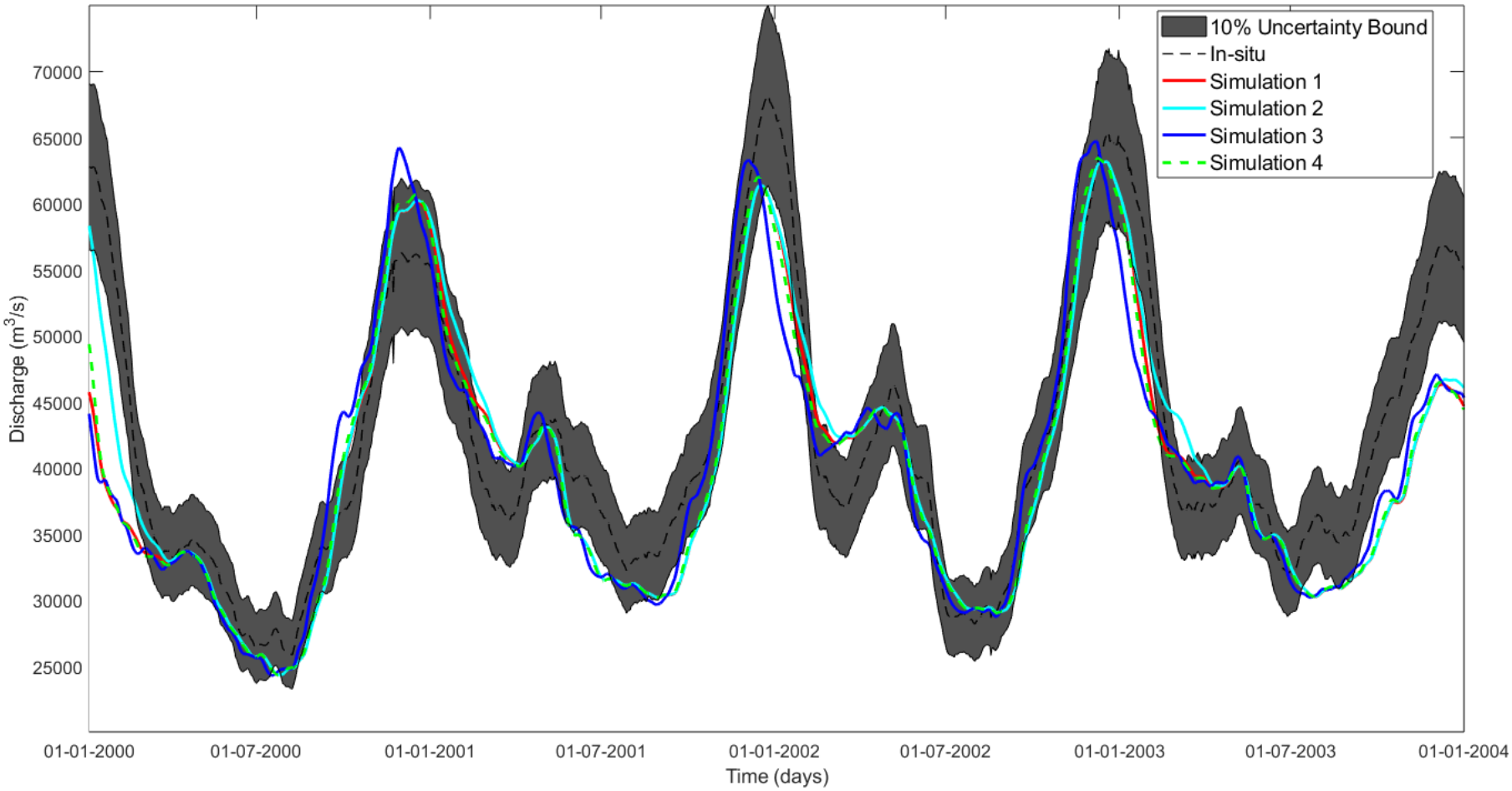

835

836 **Figure 6: Simulated and in-situ hydrographs for Kinshasa. An estimated 10% uncertainty bound for the in-situ hydrograph is shown. The first 100 days**

837 **are not included in analysis to account for any errors in initial starting conditions.**

838

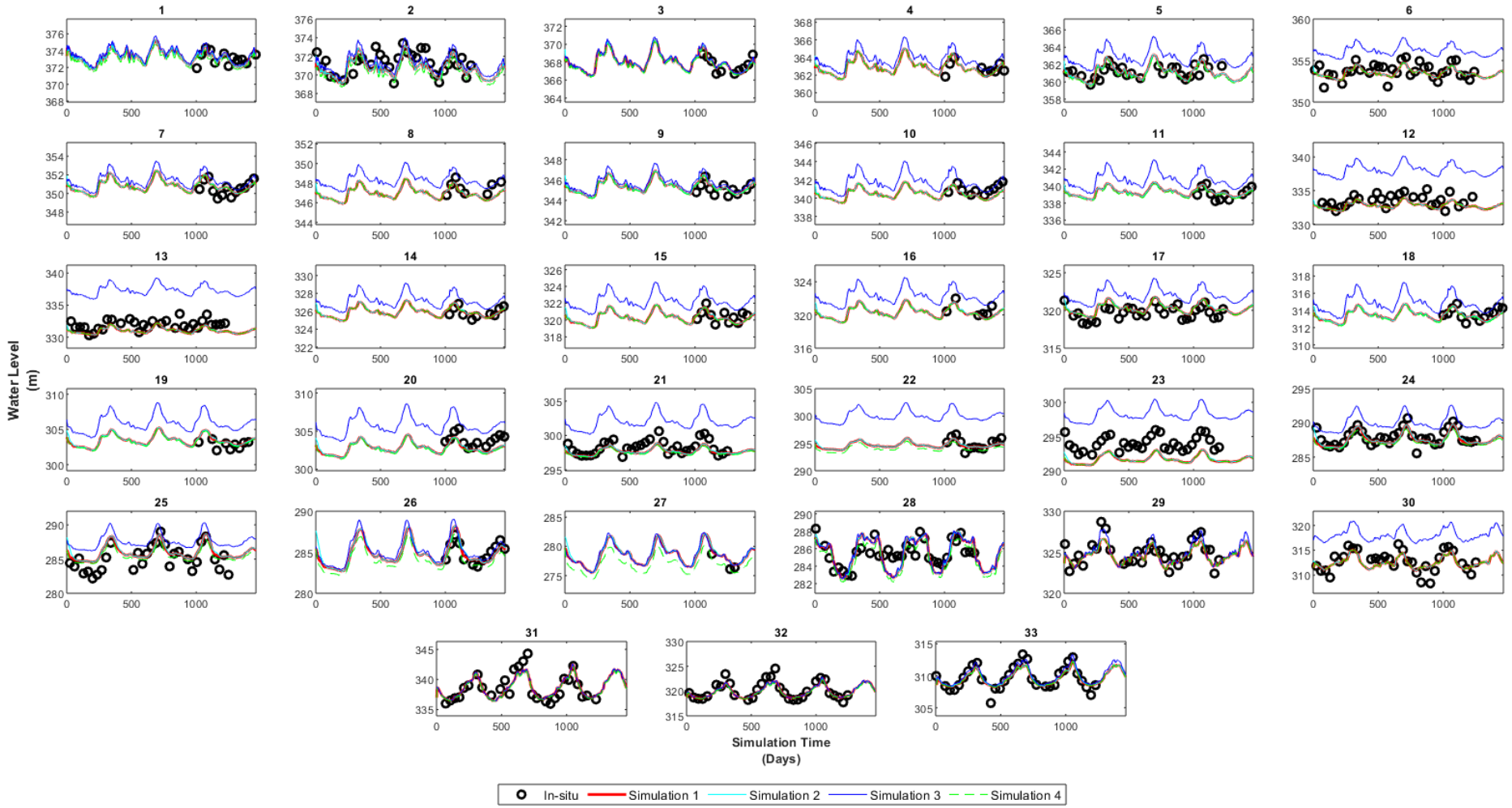

839

840 **Figure 7: Time-series of water surface elevation for the four simulations (Control [simulation 1], No Evaporation [simulation 2], Smooth Widths**

841 **[simulation 3] and No Floodplain [simulation 4]). Satellite altimetry observations are shown as black open circles.**

842

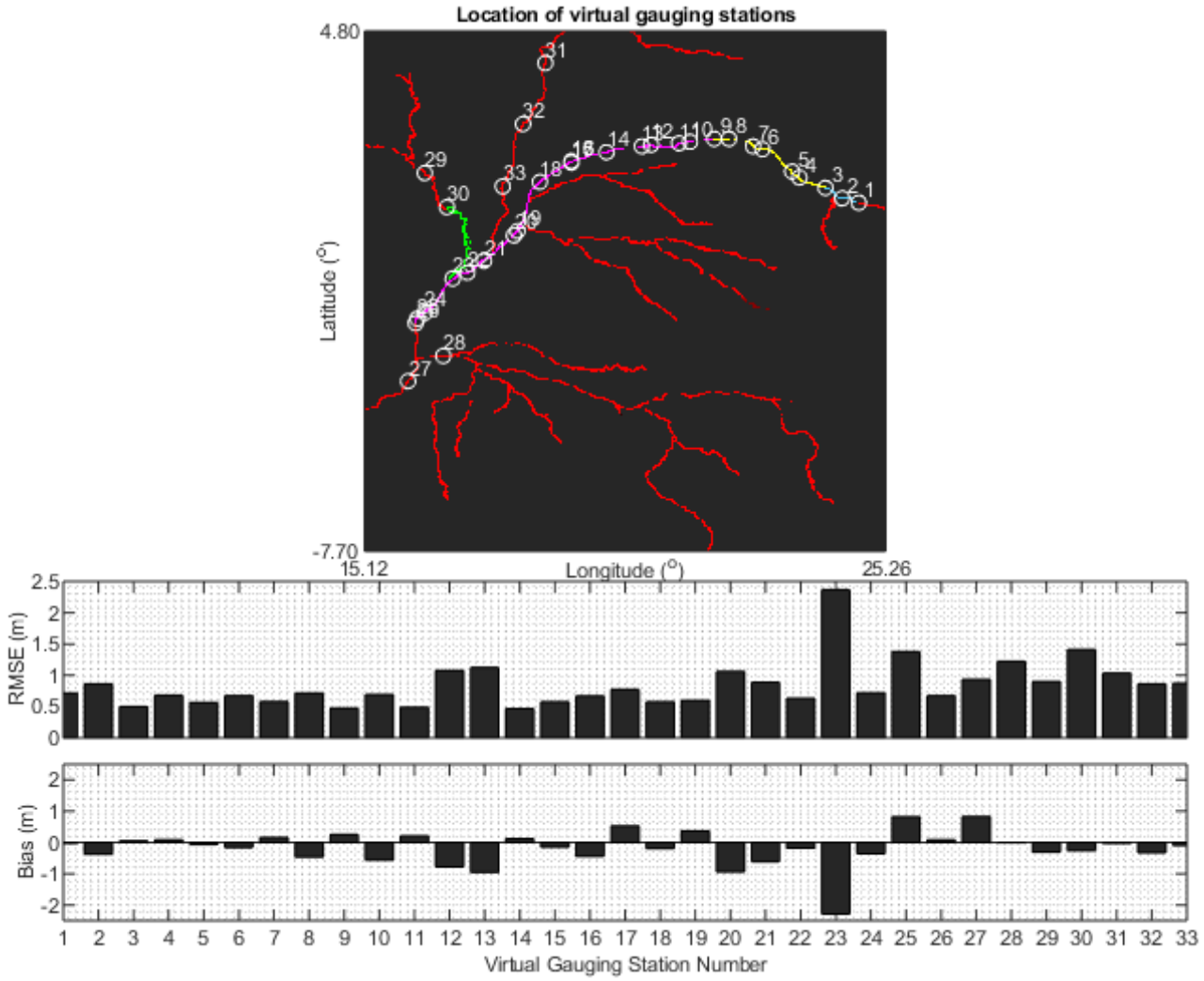

843

844 **Figure 8: Root Mean Square Error and bias for the control simulation at the virtual gauge locations obtained from satellite altimetry. location of rivers**

845 **(red), and individual floodplain units (Section 2.5) (Unit 1= blue; Unit 2 = yellow; Unit 3 = purple; and Unit 4 = green) are also shown.**

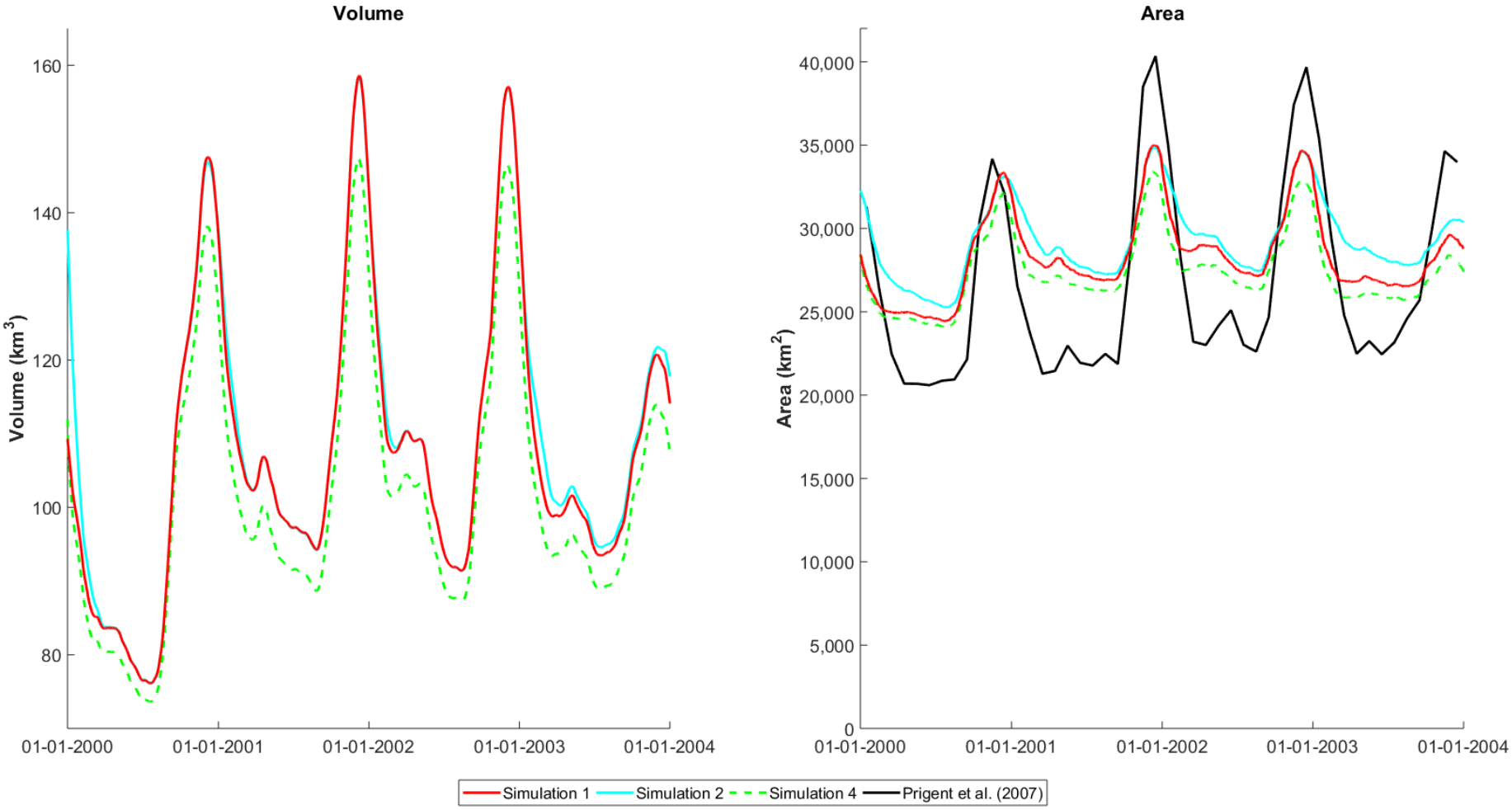

846

847 **Figure 9: Inundation Volume and Extents for three simulations (Simulation 1, Simulation 2, and Simulation 4). Observed Inundations extents obtained**

848 **from remote sensing datasets (Prigent et al., 2007) also shown. Simulation 3 not shown as no changes in inundation volumes or extents occur.**

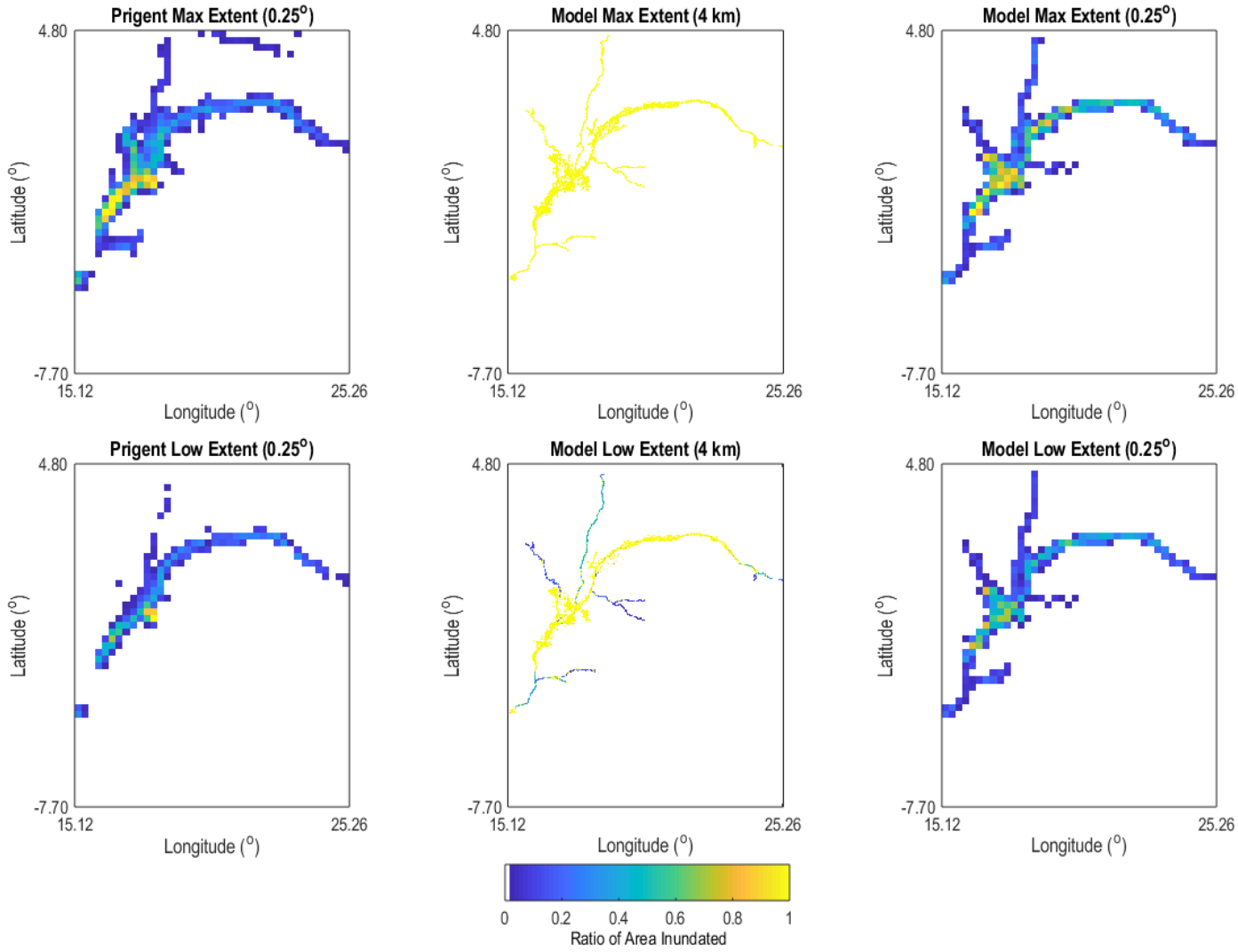

849

850 **Figure 10: Fractional Inundated Area for Maximum and Minimum Extents. Model refer to extents produced from Simulation 1, at naïve4 km resolution**

851 **and scaled to 0.25 degrees**

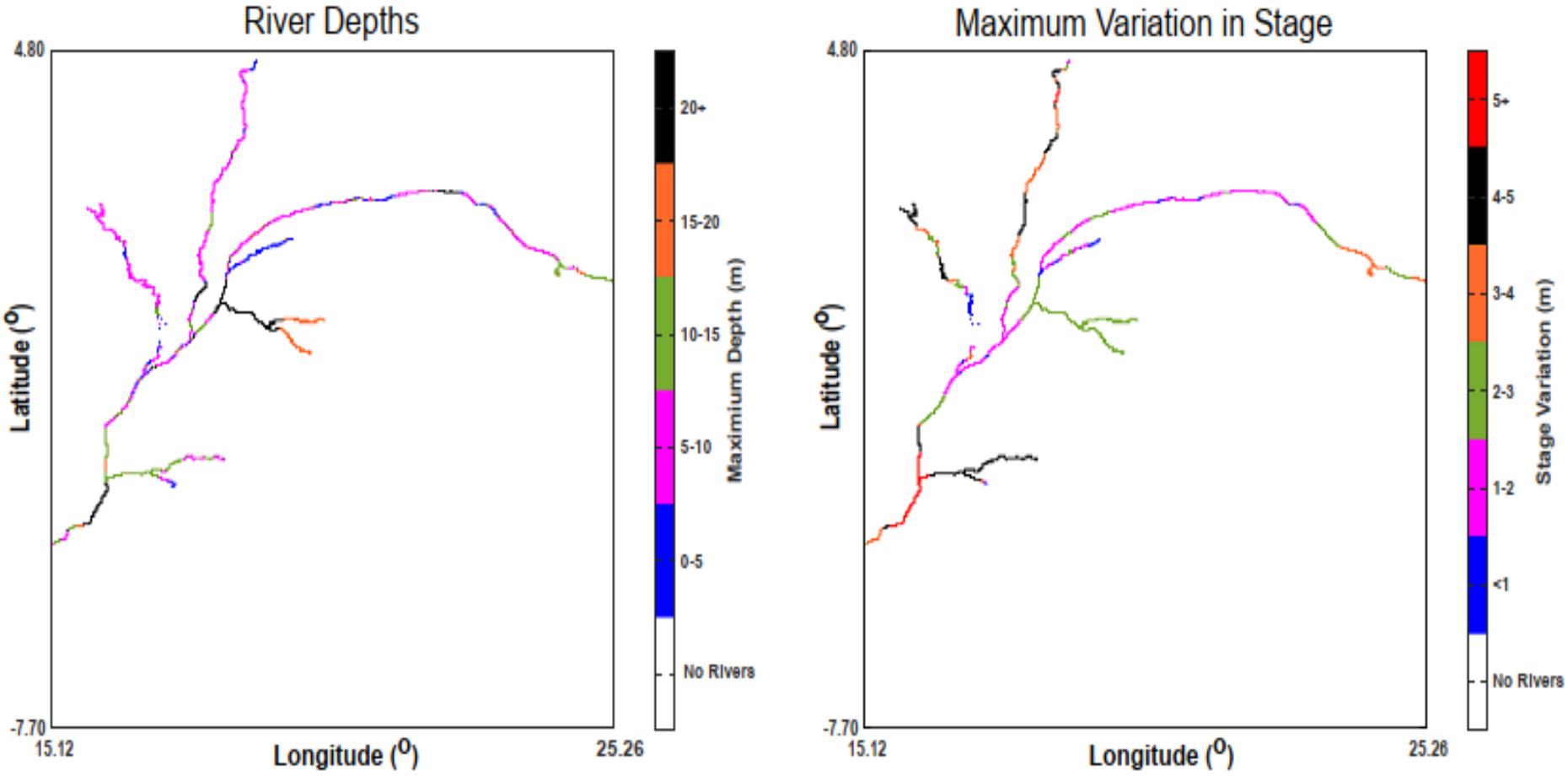

852
853

854 **Figure 11: Spatial variations in maximum river depth (left) and maximum variation in stage (right).**

855

Table 1: Overview of model simulations including model components included in each simulation.

Simulation Number	Name	Model Component			
		Floodplain Interactions	Evaporation	Constrictions	Calibrated
1	Control	✓	✓	✓	✓
2	No Evaporation	✓	-	✓	-
3	No Floodplain	-	✓	✓	-
4	Smooth Widths	✓	✓	-	-

Table 2: Comparison of the simulated and observed hydrographs at Kinshasa using the: Nash Sutcliffe Efficiency (NSE), Root Mean Square Error (m) and percentage of volume missing.

	NSE	RMSE (m^3/s)	Vol Missing %
Simulation 1	0.8386	15,083	4.024
Simulation 2	0.8373	15,142	3.315
Simulation 3	0.7897	17,216	3.1744
Simulation 4	0.8334	15,323	3.9351

Table 3: Average Root Mean Square Error (m) and Average Bias (m) between simulated and observed water levels at all Virtual Gauging Locations. Values in bracket are the RMSE and Bias when location 23 is excluded.

	RMSE (m)	Bias (m)
Simulation 1	0.842 (0.794)	-0.185 (-0.120)
Simulation 2	0.845 (0.799)	-0.162 (-0.097)
Simulation 3	2.023 (1.952)	1.735 (1.658)
Simulation 4	0.884 (0.837)	-0.393 (-0.332)

Figure captions

Figure 1: Shaded relief map of Africa showing the outline of the Congo Basin (solid red) and the model domain that has been simulated (dashed black). The red dots represent the locations of Kisangani and Kinshasa related to the model domain.

Figure 2:Schematic of Methodology, showing known variables in blue, model output in green, unknown parameters in red and calibration procedure in purple, and how they relate to the LISFLOOD-FP model.

Figure 3: Study Area showing rivers included in the hydrodynamic model and: (A) Location of discharge locations and source; and (B) ERS-2 and Envisat Virtual Gauging Locations. Variation in river width ris epresented by weight of line.

Figure 4: Hydrodynamic model schematic of (a) a typical simple 2D raster based model and (b) the sub-grid channel routine as developed by Neal et al. (2012).

Figure 5: Available in-situ observations of discharge. Missing data shown by a dashed-line (--)

Figure 6: Simulated and in-situ hydrographs for Kinshasa. An estimated 10% uncertainty bound for the in-situ hydrograph is shown. The first 100 days are not included in analysis to account for any errors in initial starting conditions.

Figure 7: Time-series of water surface elevation for the four simulations (Control [simulation 1], No Evaporation [simulation 2], Smooth Widths [simulation 3] and No Floodplain [simulation 4]). Satellite altimetry observations are shown as black open circles.

Figure 8: Root Mean Square Error and bias for the control simulation at the virtual gauge locations obtained from satellite altimetry. location of rivers (red), and individual floodplain units (Section 2.5) (Unit 1= blue; Unit 2 = yellow; Unit 3 = purple; and Unit 4 = green) are also shown.

Figure 9: Inundation Volume and Extents for three simulations (Simulation 1, Simulation 2, and Simulation 4). Observed Inundations extents obtained from remote sensing datasets (Prigent et

al., 2007) also shown. Simulation 3 not shown as no changes in inundation volumes or extents occur.

Figure 10: Fractional Inundated Area for Maximum and Minimum Extents. Model refer to extents produced from Simulation 1, at naïve4 km resolution and scaled to 0.25 degrees

Figure 11: Spatial variations in maximum river depth (left) and maximum variation in stage (right).

Figure1

Click here to download high resolution image

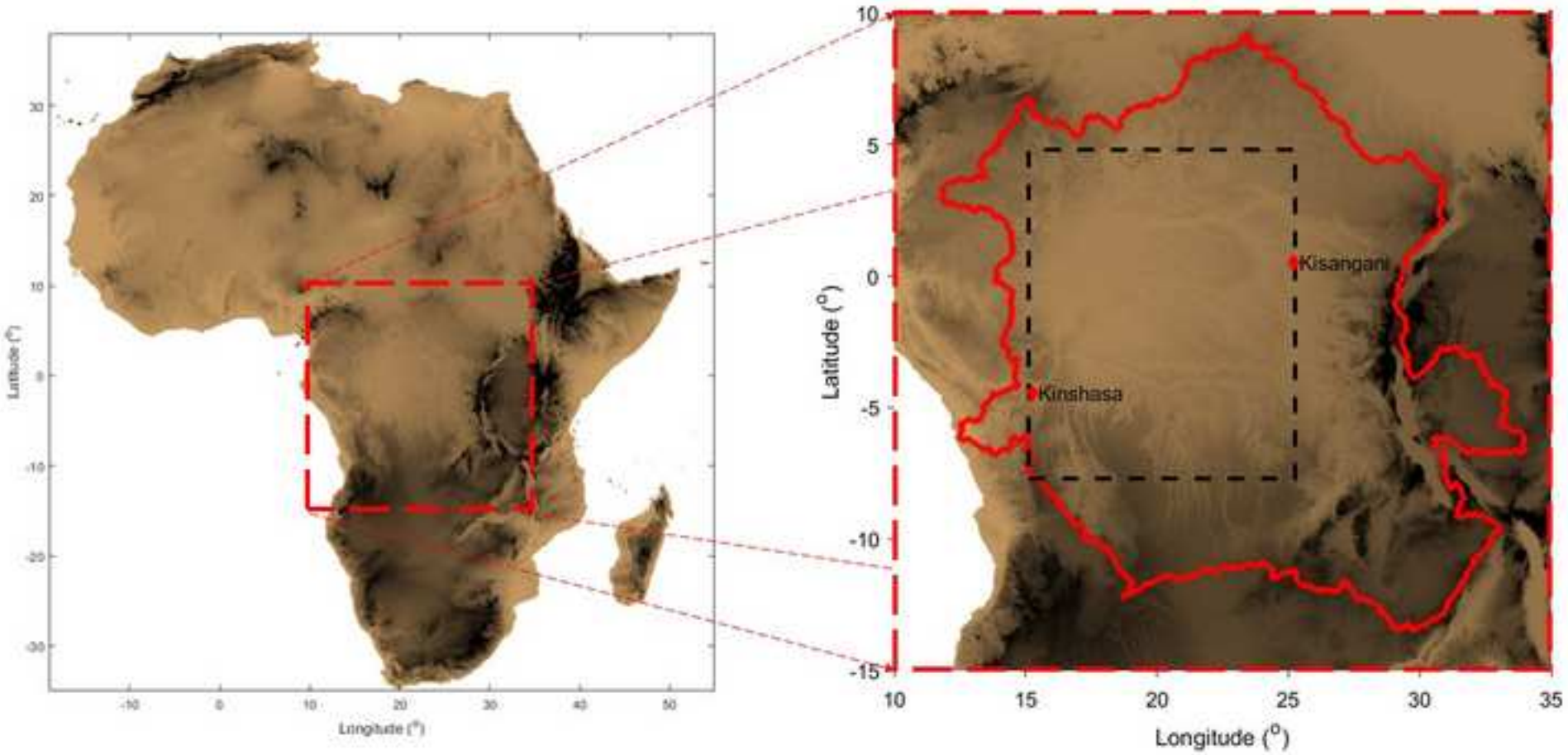

Figure2

Click here to download high resolution image

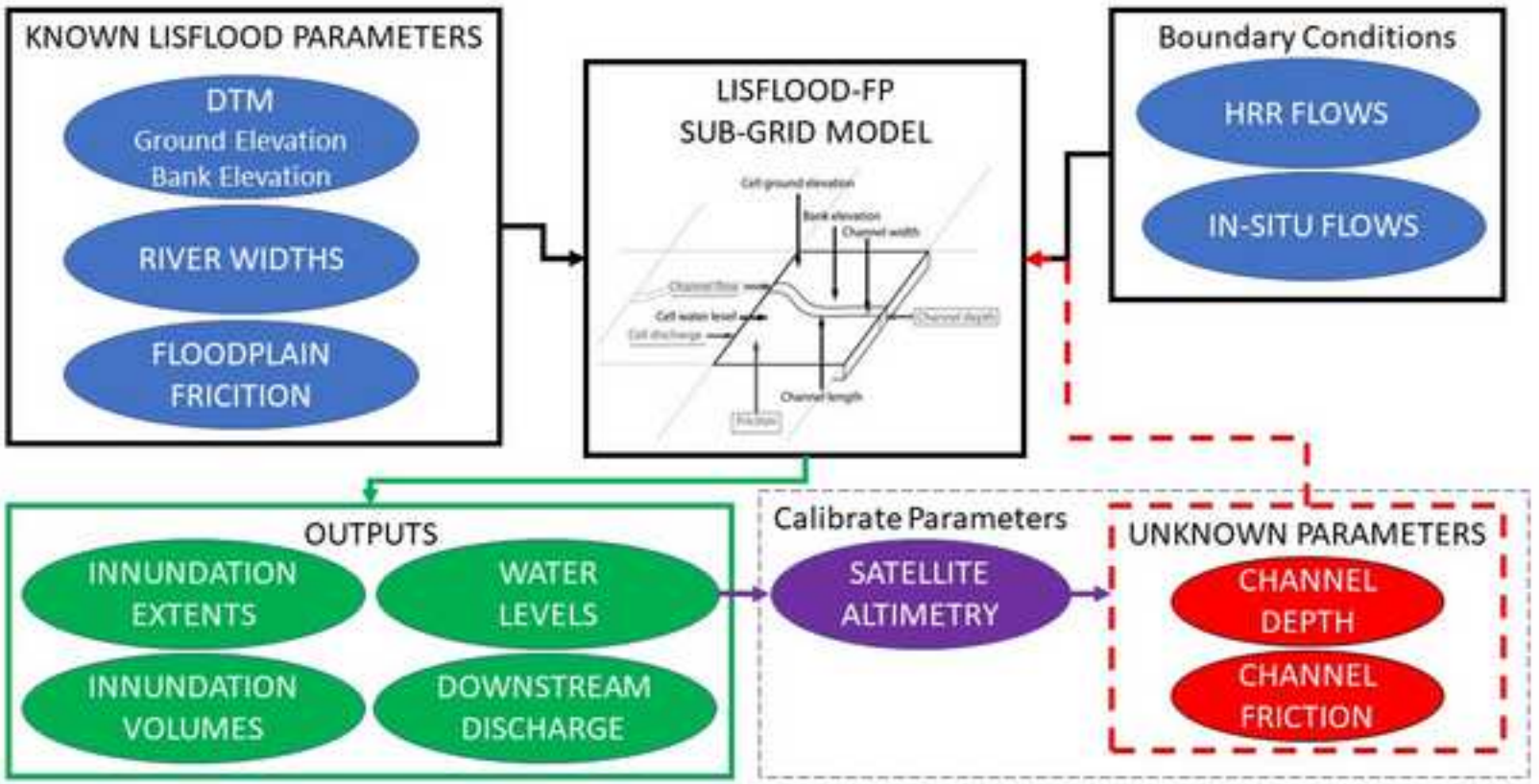

Figure3

Click here to download high resolution image

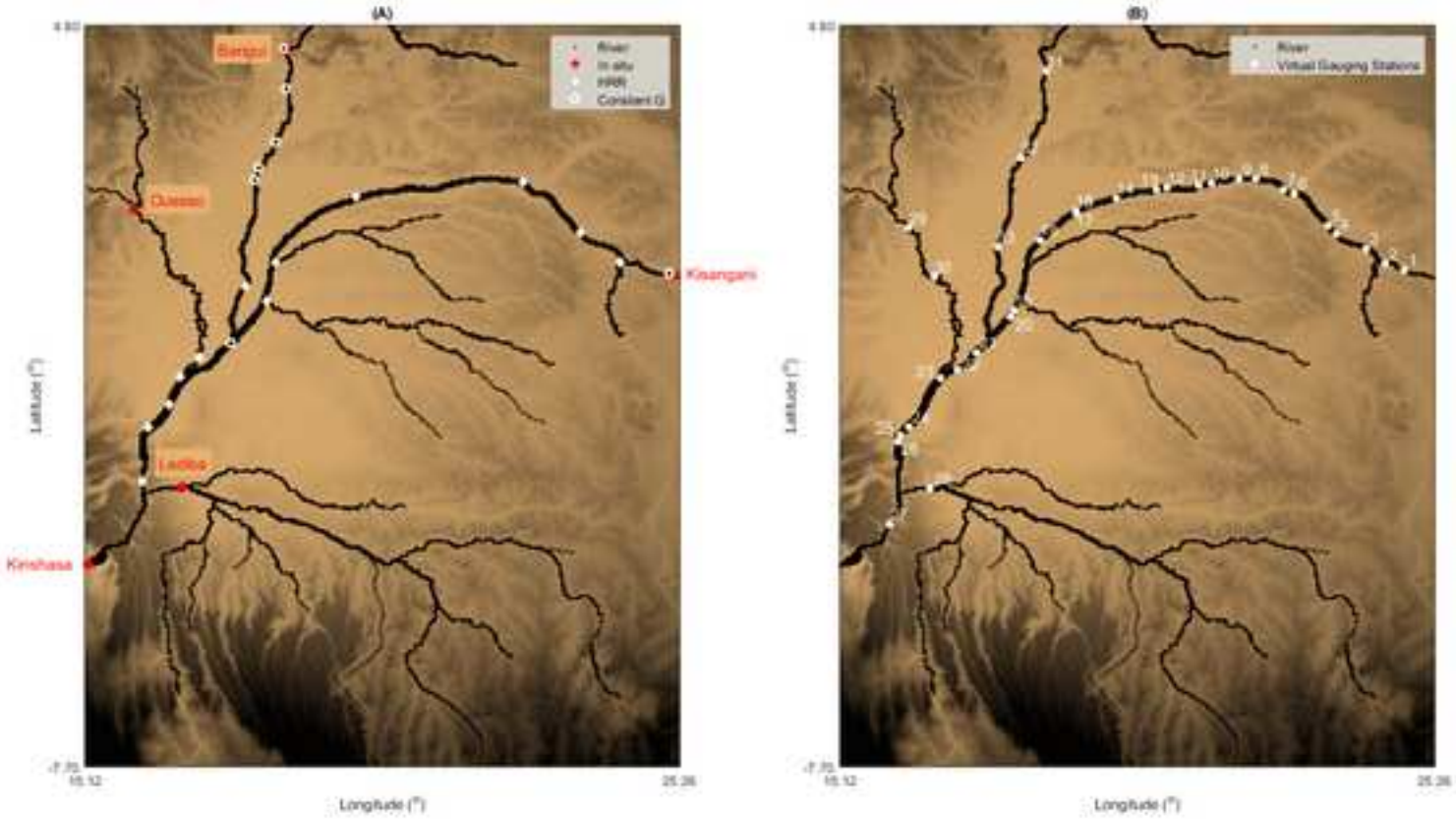

Figure4

Click here to download high resolution image

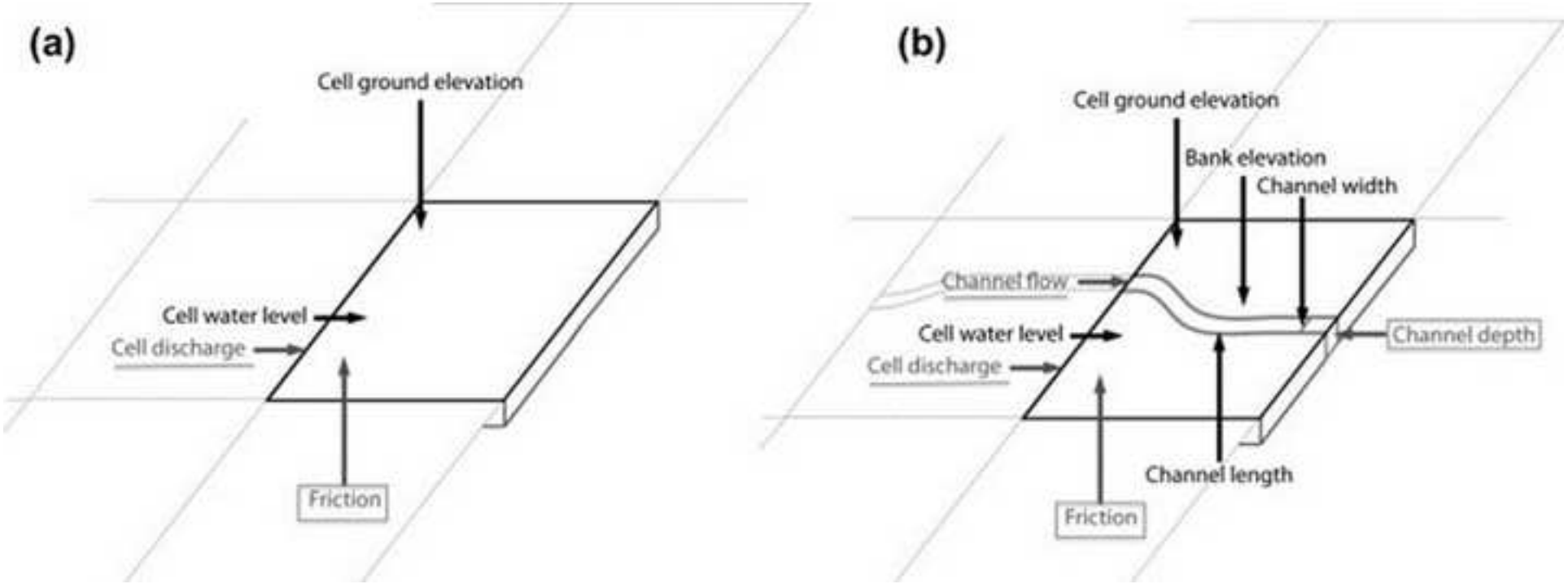

Figure5

Click here to download high resolution image

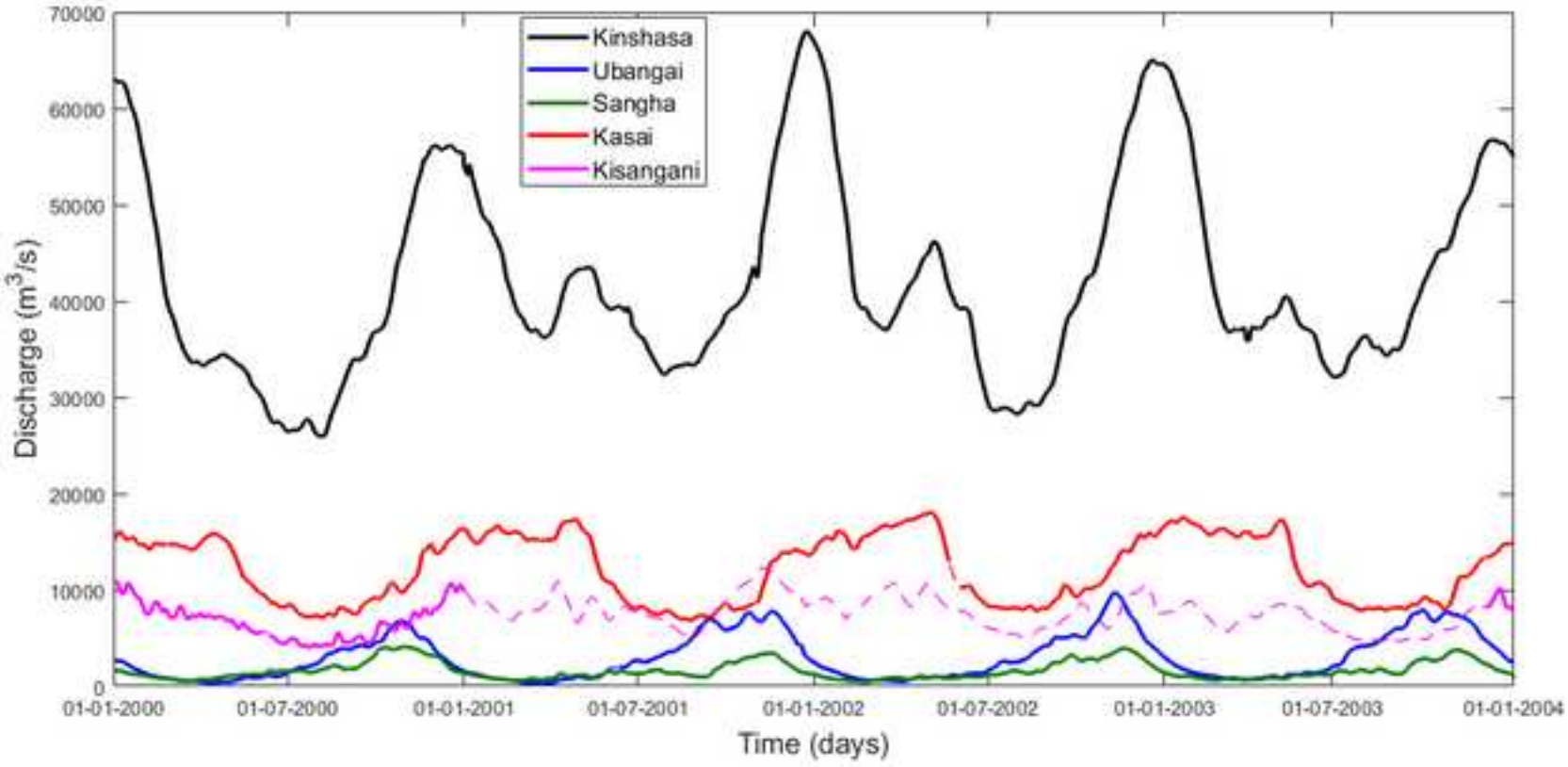

Figure6

Click here to download high resolution image

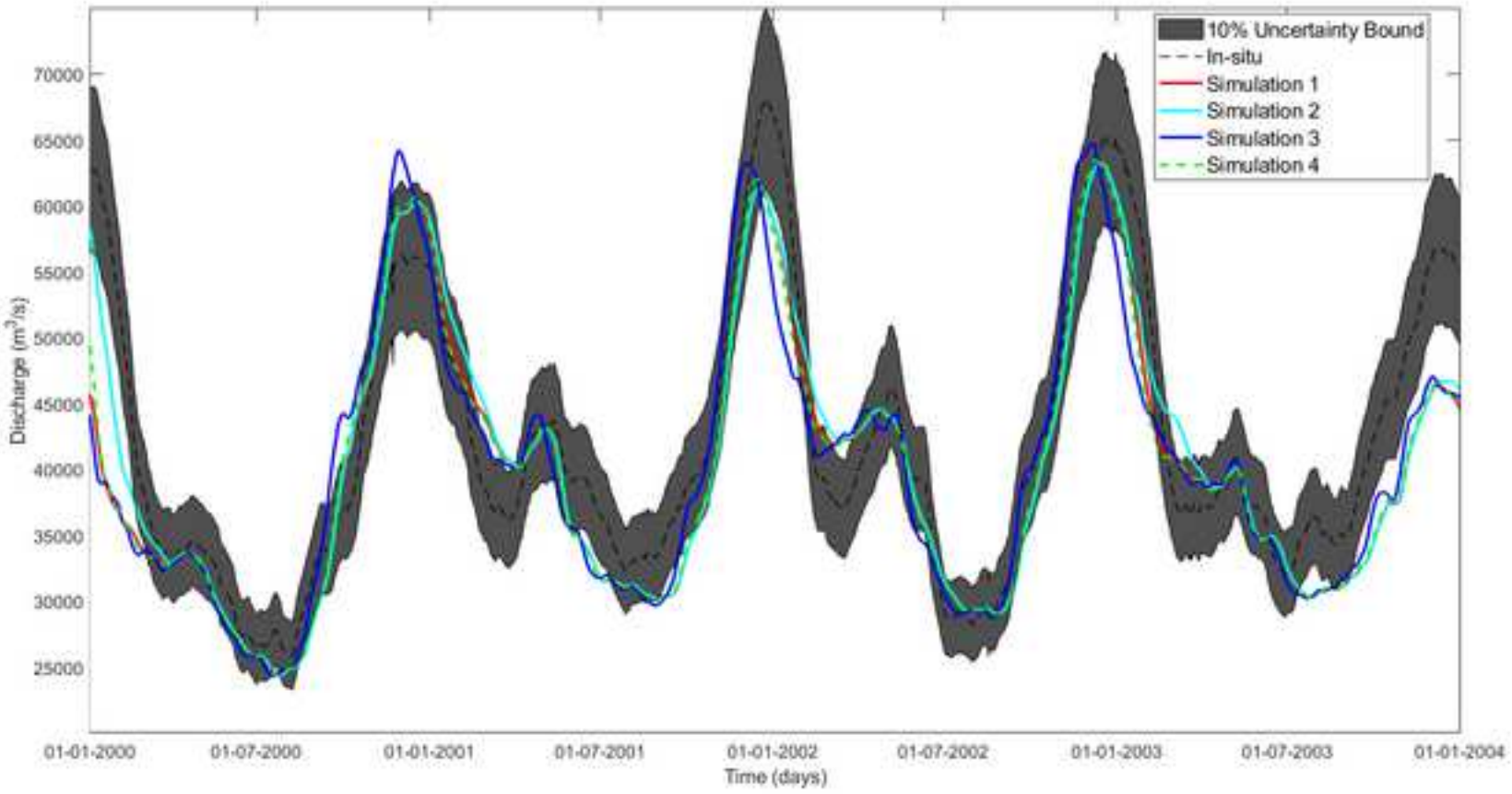

Figure7

Click here to download high resolution image

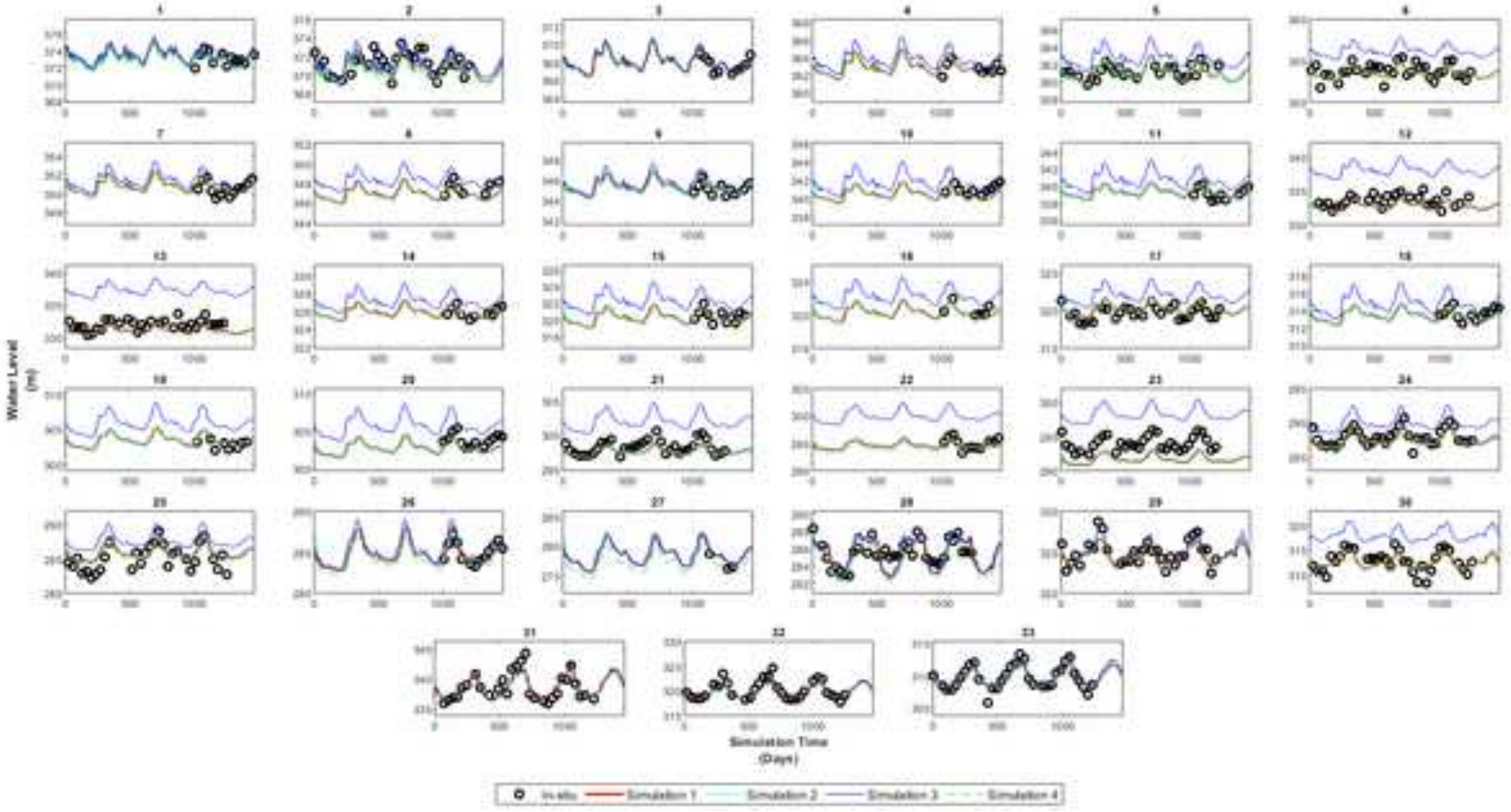

Figure8

Click here to download high resolution image

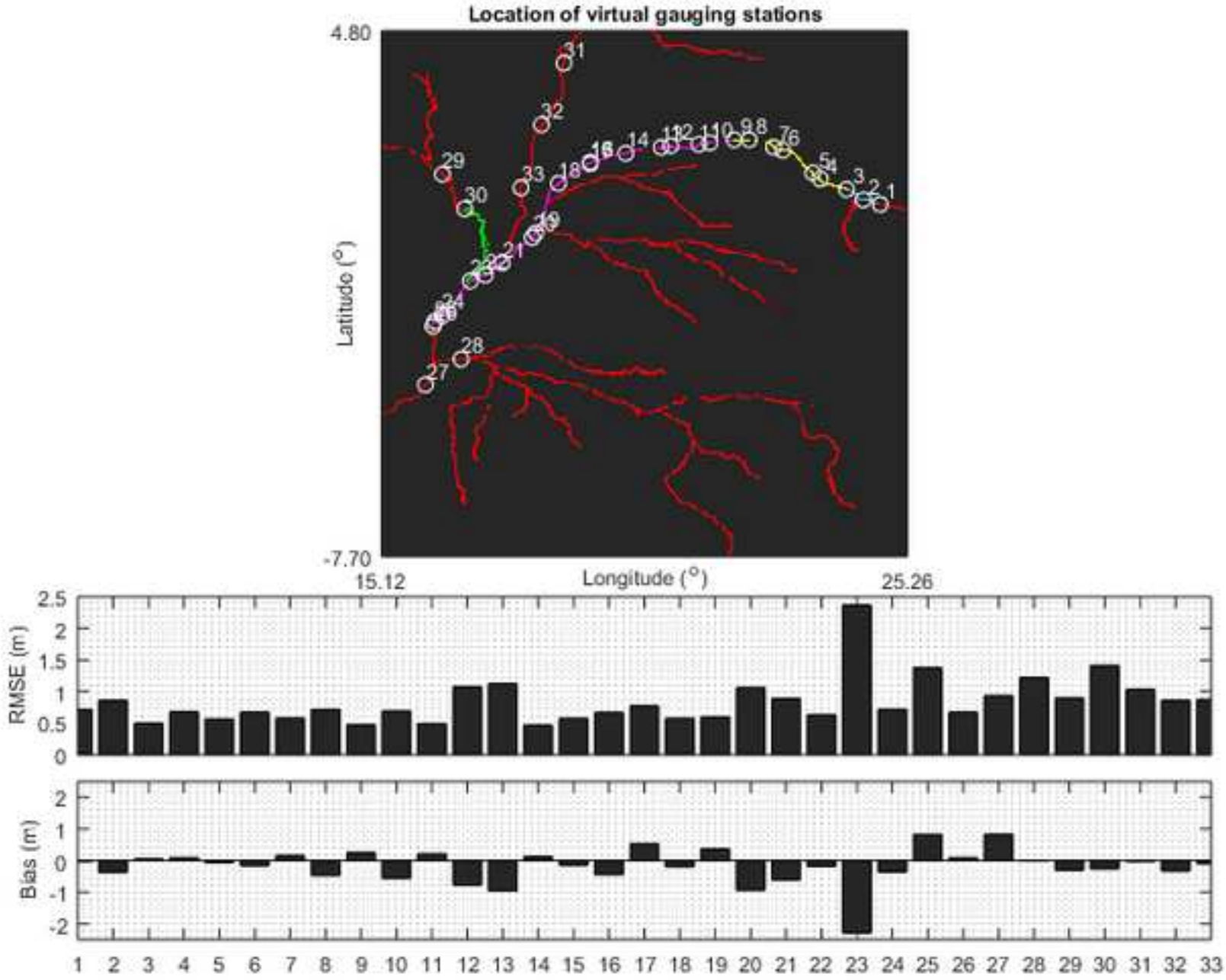

Figure9

Click here to download high resolution image

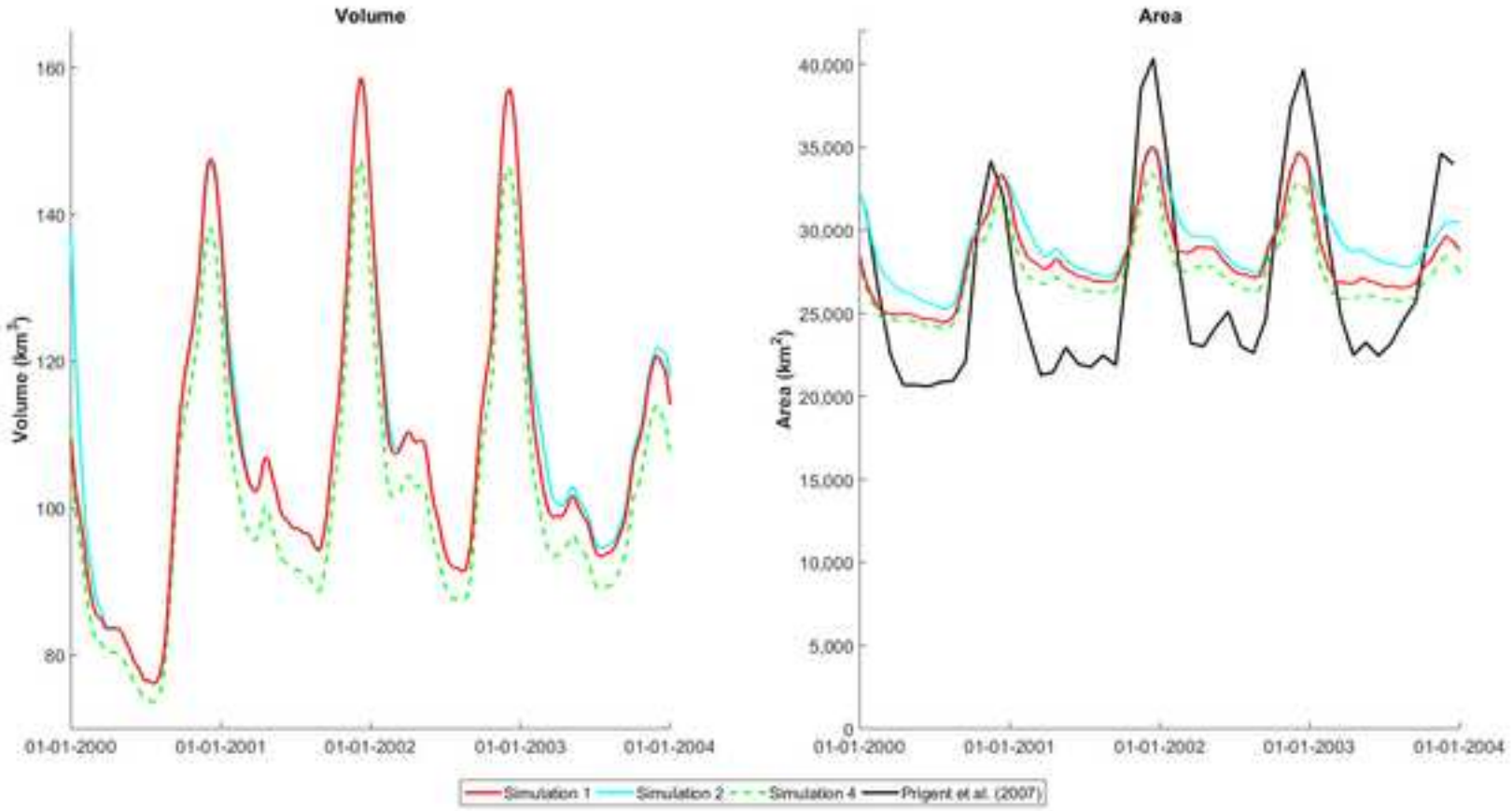

Figure10

Click here to download high resolution image

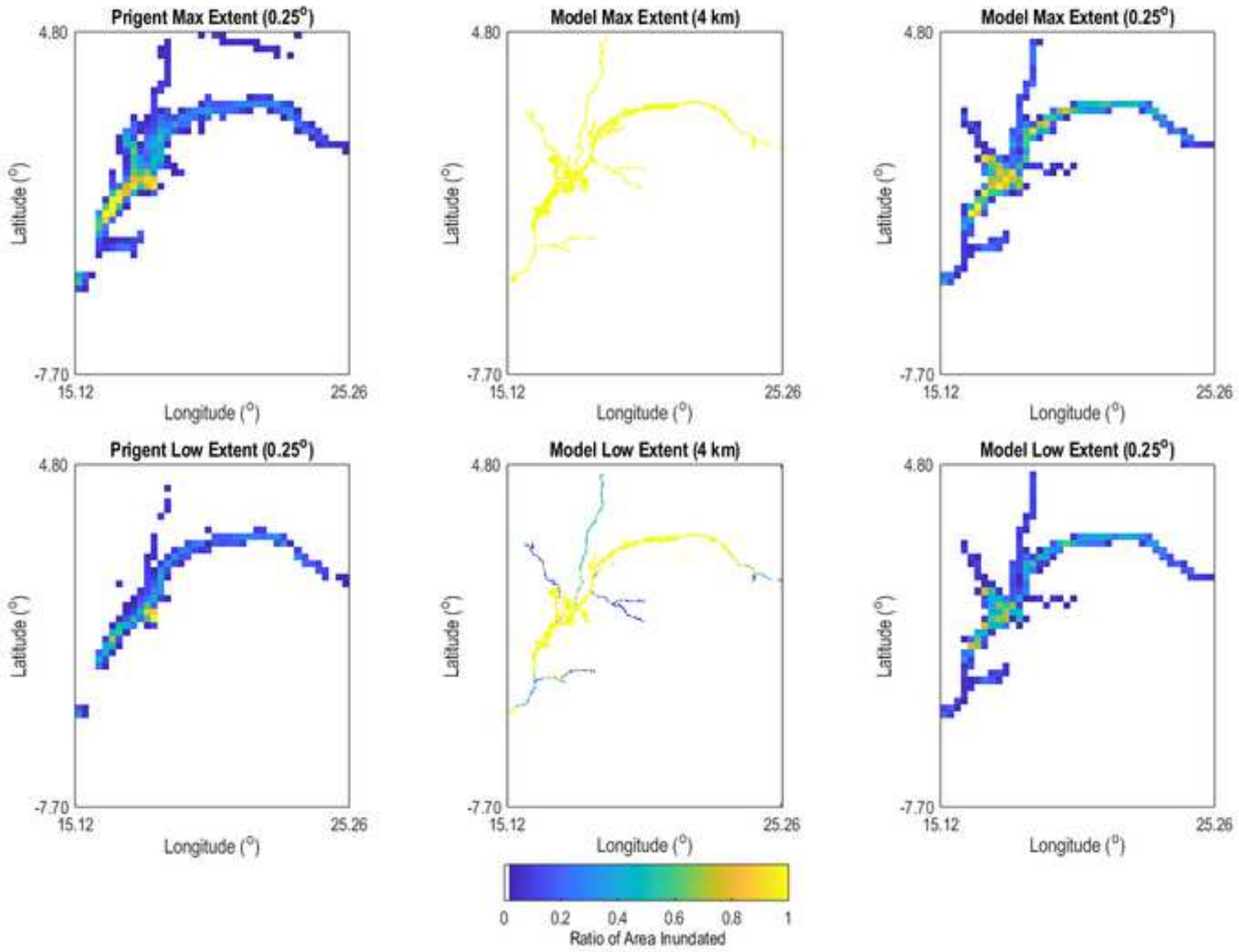

figure10_sept.tif

Figure11

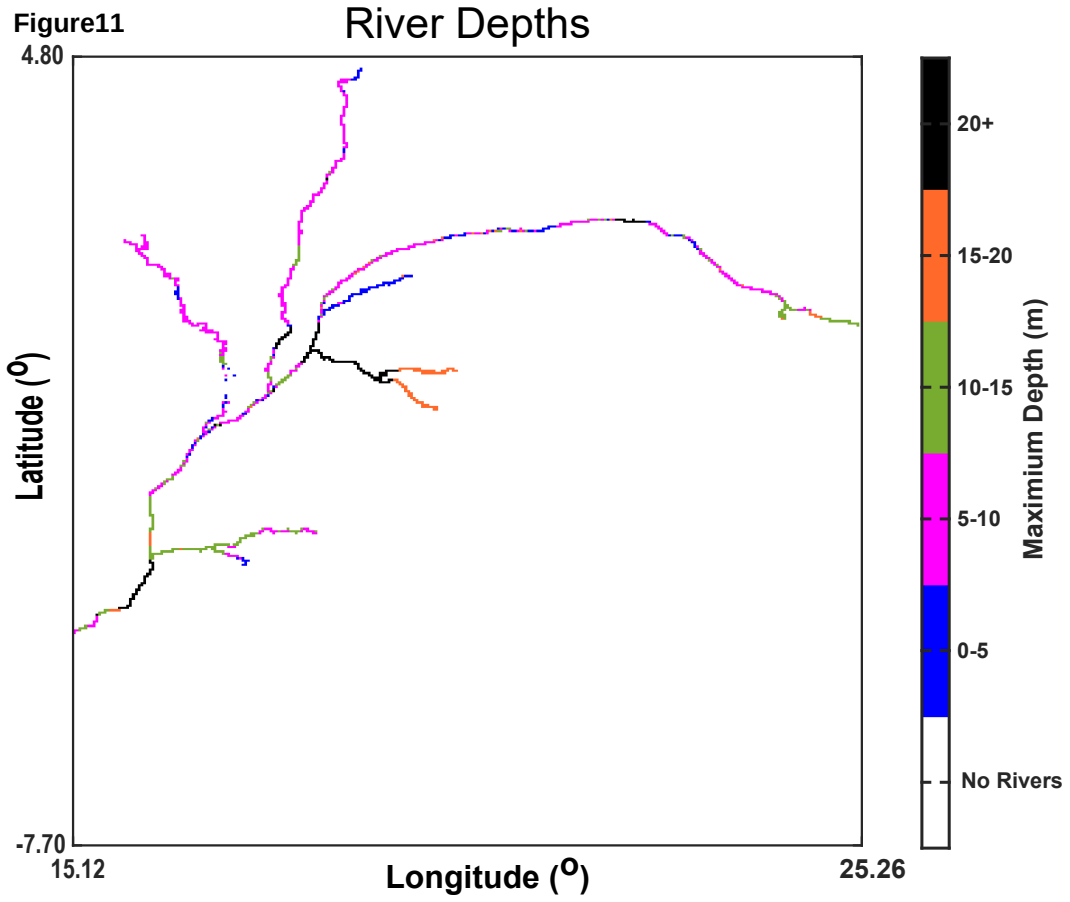
River Depths
4.80
-7.70
15.12
25.26
Latitude (O)
Longitude (O)
20+
15-20
10-15
5-10
0-5
No Rivers
Maximium Depth (m)

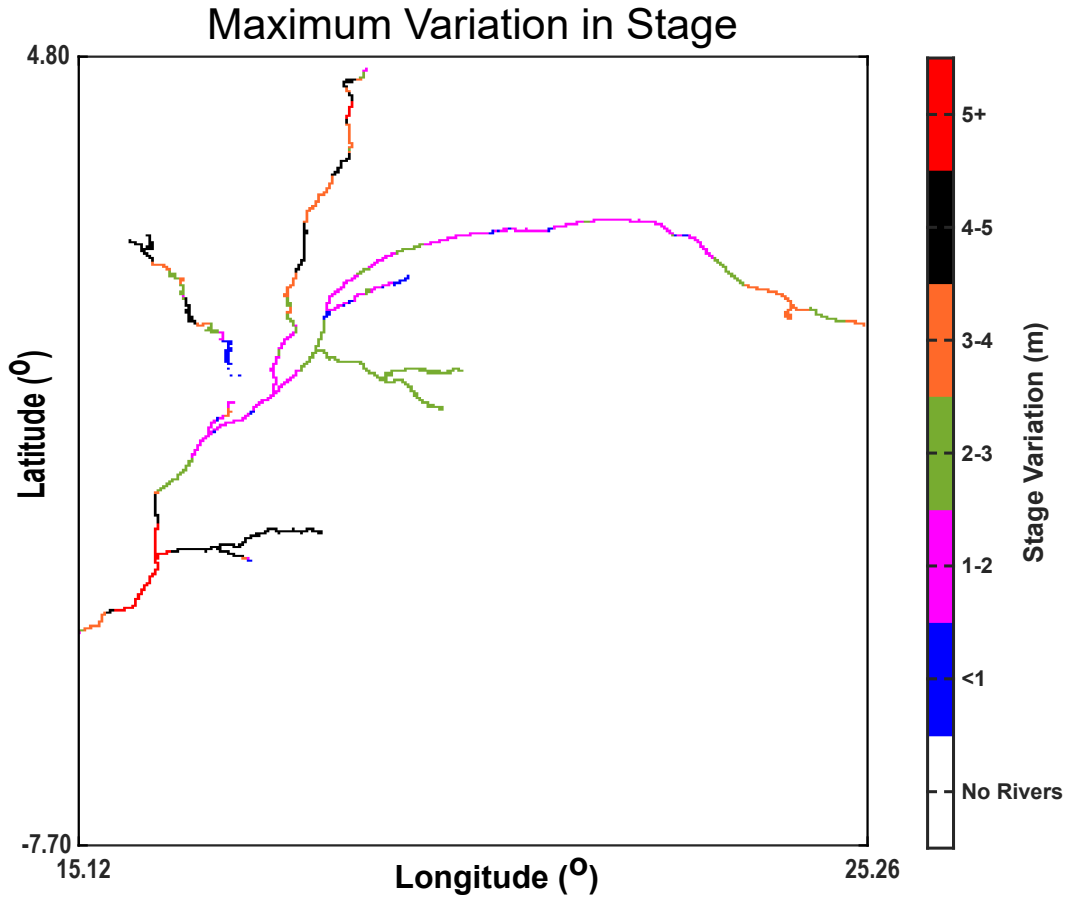
Maximum Variation in Stage
4.80
-7.70
15.12
25.26
Latitude (O)
Longitude (O)
5+
4-5
3-4
2-3
1-2
<1
No Rivers
Stage Variation (m)

Table1
Click here to download Table: Table1.docx

Table 1: Overview of model simulations including model components included in each simulation.

Simulation Number	Name	Model Component			
		Floodplain Interactions	Evaporation	Constrictions	Calibrated
1	Control	✓	✓	✓	✓
2	No Evaporation	✓	-	✓	-
3	No Floodplain	-	✓	✓	-
4	Smooth Widths	✓	✓	-	-

Table2
Click here to download Table: Table2.docx

1 **Table 1: Comparison of the simulated and observed hydrographs at Kinshasa using the: Nash**

2 **Sutcliffe Efficiency (NSE), Root Mean Square Error (m) and percentage of volume missing.**

	NSE	RMSE (m^3/s)	Vol Missing %
Simulation 1	0.8386	15,083	4.024
Simulation 2	0.8373	15,142	3.315
Simulation 3	0.7897	17,216	3.1744
Simulation 4	0.8334	15,323	3.9351

3

Table3
Click here to download Table: Table3.docx

Table 1: Average Root Mean Square Error (m) and Average Bias (m) between simulated and observed water levels at all Virtual Gauging Locations. Values in bracket are the RMSE and Bias when location 23 is excluded.

	RMSE (m)	Bias (m)
Simulation 1	0.842 (0.794)	-0.185 (-0.120)
Simulation 2	0.845 (0.799)	-0.162 (-0.097)
Simulation 3	2.023 (1.952)	1.735 (1.658)
Simulation 4	0.884 (0.837)	-0.393 (-0.332)